Lead Halide Perovskite Nanocrystals: Room Temperature Syntheses towards Commercial Viability

Alasdair A. M. Brown,[1,2,3,4,] Bahulayan Damodaran,[4] Liudi Jiang,[1] Ju Nie Tey,[3] Suan Hui Pu,[1,2] Nripan Mathews,[4,5] and Subodh G. Mhaisalkar.[4,5,*]*

[1] *Faculty of Engineering and Physical Sciences, University of Southampton, University Road, Southampton, SO171BJ, United Kingdom*

[2] *University of Southampton Malaysia, Iskandar Puteri, 79200, Johor, Malaysia*

[3] *Singapore Institute of Manufacturing Technology, Agency for Science and Technology Research (A*STAR), 73 Nanyang Drive, Singapore, 637662, Republic of Singapore*

[4] *Energy Research Institute at NTU (ERI@N), Research Techno Plaza, Nanyang Technological University, 50 Nanyang Drive, Singapore, 637553, Republic of Singapore*

[5] *School of Materials Science and Engineering, Nanyang Technological University, 50 Nanyang Drive, Singapore, 637553, Republic of Singapore*

*E-mail: subodh@ntu.edu.sg; aam.brown@soton.ac.uk

Abstract

In this Progress Report, we assess recent improvements to the room temperature syntheses of lead halide perovskite nanocrystals ($APbX_3$, X = Cl, Br, I), focusing on various aspects which influence the commercial viability of the technology. Perovskite nanocrystals can be prepared easily from low cost precursors under ambient conditions, yet they have displayed near-unity photoluminescence quantum yield with narrow, highly tuneable emission peaks. In addition to their impressive ambipolar charge carrier mobilities, these properties make lead halide perovskite nanocrystals very attractive for LED applications. However, there remain many practical hurdles to commercialization. We review recent developments in room temperature synthesis and purification protocols, closely addressing the suitability of particular techniques for industry. We follow this by exploring the wide range of ligands deployed on perovskite nanocrystal surfaces, analyzing their impact on colloidal stability, as well as LED efficiency. Based on these observations, we then provide our perspective on important future research directions that could expedite the industrial adoption of perovskite nanocrystals.

1. Introduction

The last decade has seen both the emergence of lead halide perovskites as active optoelectronic materials,[1–3] and their unprecedented rapid development for an enormous range of applications.[4] The most intense focus has been on solar cells,[5–8] but there has also been substantial research on perovskite-based light emitting diodes (LEDs),[9–13] transistors,[14,15] lasers,[12,16,17] gas sensors,[4,18] and photodetectors.[19–21] The versatility of lead halide perovskites is attributable to their plethora of desirable properties; they exhibit long carrier diffusion lengths,[22,23] high absorption coefficients,[1] facile band-gap tuneability[24] and exceptional defect tolerance.[25,26] Defect tolerance is an especially attractive property as it makes solution-processing in ambient conditions a viable prospect. Combined with the relatively low cost of perovskite precursor salts, perovskite-based optoelectronics possess substantial commercial appeal.

Lead halide perovskites possess a cuboctahedral structure of the form $APbX_3$, which describes a cuboidal unit cell with an A cation at its center, surrounded by 8 corner-sharing $[PbX_6]^{4-}$ octahedra.[27] The A site is typically composed of methylammonium (MA), formamidinium (FA) or cesium (Cs) ions, while halides (exclusively chloride, bromide or iodide) occupy the X sites. The defect tolerance of this structure originates from the benign nature of thermodynamically viable trap states.[25,28] Interstitial and anti-site defects, and Pb^{2+} vacancies, are highly unlikely to form, thus in reality only X site vacancies are observed. These halide vacancies only manifest as in-band or shallow traps states,[29,30] thus ideal optoelectronic properties can be maintained with defect densities that would render other materials useless.

Defect tolerance is especially beneficial for the commercial prospects of perovskite nanocrystals, whose surfaces are essentially planes of vacancies. While the nanocrystal surface must be well-passivated to yield useful properties, the desorption of some surface-passivating ligands has a far less debilitating effect on perovskites than other types of nanocrystal, as the induced defect states are mainly delocalized in the valence band. As a result, perovskite nanocrystals still exhibit excellent optoelectronic properties when synthesized, processed and deposited in ambient conditions.

The spatial charge confinement afforded by the dimensions of nanocrystals enhances the photoluminescence quantum yield (PLQY), which is a particularly crucial parameter for light emitting applications.[31,32] The dimensions of the nanocrystal are maintained by a shell of organic ligands, with functional groups at their head to bind to the nanocrystal surface, and long hydrocarbon tails to both hinder crystal agglomeration and enable dispersion in organic solvents.[33,34] Thus, high-efficiency LEDs have been obtained from perovskite nanocrystal inks through solution-processing techniques under ambient conditions.[35–37]

The properties of the organic ligands used have an enormous influence on the properties of the nanocrystal ink and resulting electronic devices. The nature of the interaction between the ligand binding

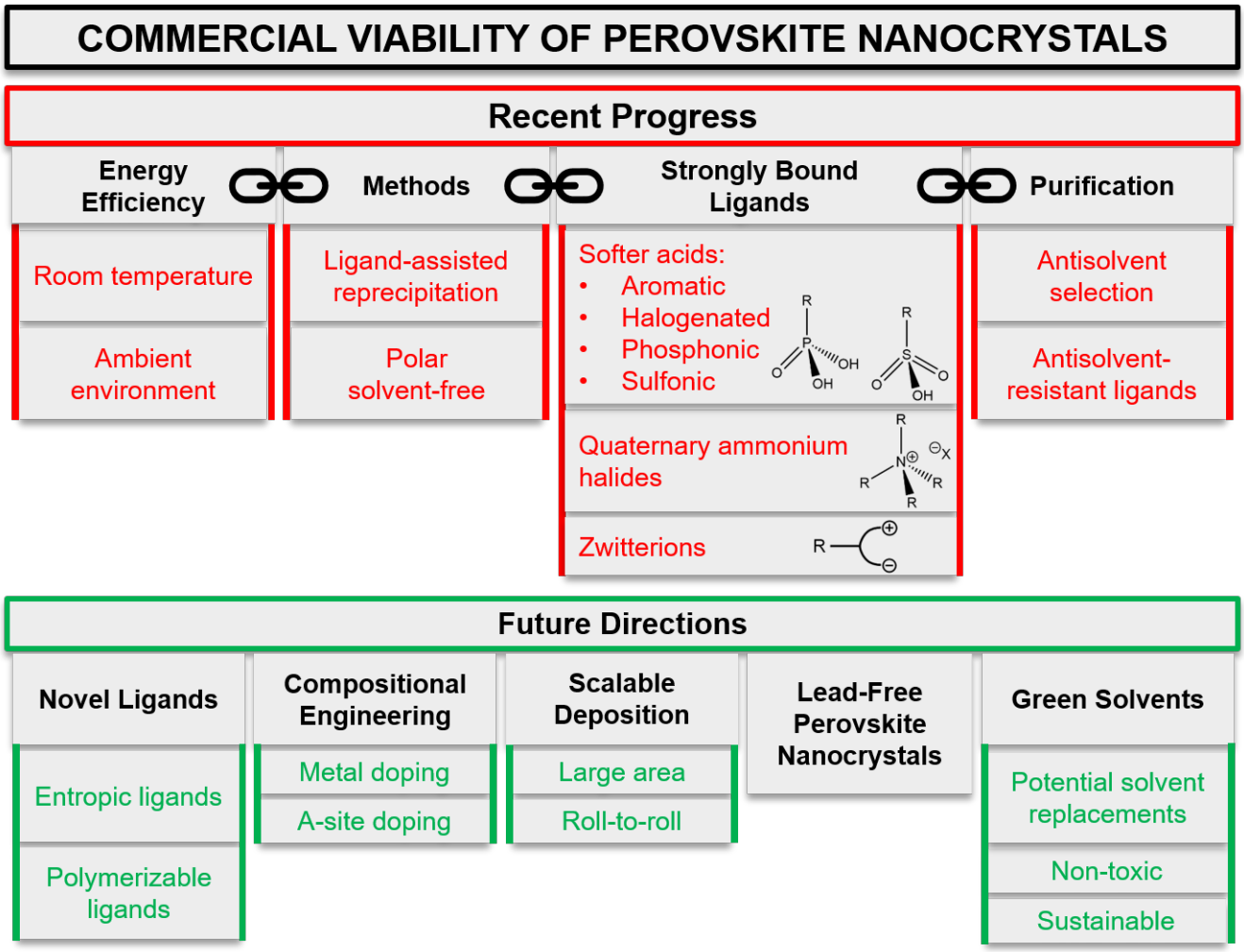

Scheme 1. An outline of the research covered in this Progress Report. **Recent Progress** summarizes the four key areas of development towards commercially viable perovskite nanocrystals discussed herein, all of which are closely linked. **Future Directions** shows promising routes for further improvement, and their main components.

group and the nanocrystal surface is crucial to the efficacy and stability of surface defect passivation.[38,39] The length, bulk and branching of the ligand tail strongly affects the colloidal stability of the nanocrystals and their conductivity when deposited as thin-films for electronic devices.[40–42] Furthermore, the one-pot nature of the colloidal synthesis means that the impact of purification processes, which are necessary to remove reaction by-products and excesses, must also be considered.[43–45]

Beyond the properties of specific ligands, the synthetic methodology employed also influences the commercial attraction of perovskite nanocrystals. Most commonly, high-temperature, air-free "hot-injection" syntheses are employed, which are challenging to scale up.[46] Room temperature processes, especially those conducted without environmental controls, present a far more economically attractive proposition.[41,47] Other relevant factors include synthetic reproducibility and the suitability of solvents and deposition methods for large-scale processing, particularly the identification of suitable green solvents.

In this Progress Report, we will evaluate recent key developments of perovskite nanocrystal syntheses, focusing particularly on the methodology and the efficacy of the ligand chemistry reported. We will assess advances that address the many aspects which govern the future suitability of this technology for industrial processing and comment on potential important research directions. We will identify promising routes to accelerate the progress towards the adoption of perovskite nanocrystals by the consumer electronics industry.

2. Room Temperature Perovskite Nanocrystal Syntheses

2.1. Ligand Assisted Reprecipitation (LARP)

The most common room temperature synthesis method is ligand-assisted reprecipitation (LARP). It is very simple, requiring only basic wet chemistry apparatus: a beaker and a syringe. It is therefore inherently scalable, and overwhelmingly more appealing to industry from financial, energy and complexity perspectives.

In the early LARP approaches, the precursor halide salts (i.e. AX and PbX_2) were dissolved stoichiometrically in a polar solvent, normally dimethylformamide (DMF) or dimethyl sulfoxide (DMSO). This solution was injected into a solvent that it is miscible with, but in which the constituent perovskite ions are much less soluble (usually toluene), creating a supersaturated state. Consequently, the perovskite structure immediately crystallizes.[48] In order to limit crystal growth to the nanoscale, organic ligands are added to either solvent prior to nucleation. The long organic chains of the ligands attached to adjacent crystals repel one another, deterring crystal aggregation, while also enabling the stable colloidal dispersion of the nanocrystals in non-polar organic solvents.

2.1.1. Organic-Inorganic Perovskite Nanocrystals

The first LARP synthesis of perovskite nanocrystals (NCs) was the preparation of $MAPbX_3$ NCs by Zhang et al.[48] They utilized two ligands, oleic acid and octylamine, which they added into their DMF precursor solution, as shown in Figure 1. They discovered that the amine ligand controlled the reaction kinetics, and therefore the size distribution of particles formed. Meanwhile, the longer oleic acid ligand was responsible for colloidal stability of the NCs.

Shortly after this paper, there followed several other LARP syntheses of $MAPbX_3$ and $FAPbX_3$ NCs, following similar protocols.[49–52] However, the thermal and environmental stability of these materials are compromised by their volatile organic cations.[53,54] All-inorganic $CsPbX_3$ typically offers much higher stability, and therefore represents a far more realistic option for commercial applications.[55–58] An important caveat to this concerns $CsPbI_3$, whose phase instability has hindered progress, such that stable $CsPbI_3$ nanocrystals have yet to be achieved through room temperature syntheses.

This Progress Report will focus on cesium-based perovskite nanocrystals. Despite this, pertinent

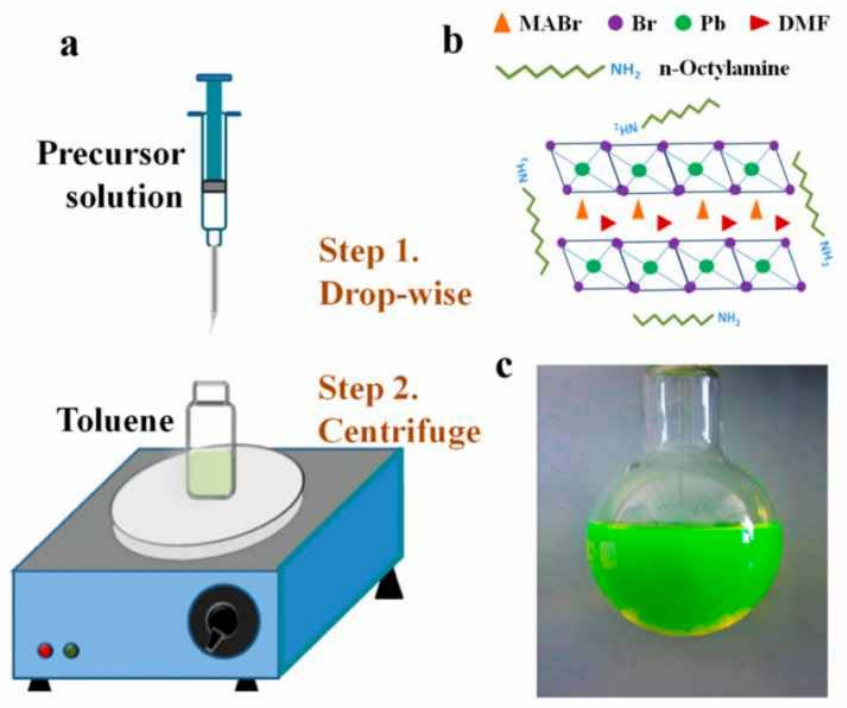

Figure 1. The first room temperature synthesis of perovskite nanocrystals: (a) synthesis setup, where the perovskite precursor solution is injected into a stirring volume of toluene, (b) the starting materials and (c) the resulting $MAPbBr_3$ nanocrystal solution. Reproduced with permission from Ref.[48] Copyright 2015 American Chemical Society.

advances made using MA or FA-based NCs will be discussed where the findings are obviously transferable to Cs-based NCs, such as novel ligand systems. We will apply the same logic for reports using high temperature syntheses. For more general overviews of perovskite nanocrystal syntheses using different cations, and high temperature syntheses, we direct readers towards other extensive recent reviews.[28,59–62]

2.1.2. Inorganic Perovskite Nanocrystals

The first use of LARP for $CsPbX_3$ NC synthesis was reported by Li et al. in 2016.[63] They added oleic acid and oleylamine, the same ligands typically used for early hot-injection approaches, to the halide salt precursor in DMF, as shown in Figure 2. They obtained NCs with PLQY > 70 % for various emission wavelengths between 478 and 640 nm ($CsPbClBr_2$ to $CsPbBrI_2$), with a maximum PLQY of 95 % for the pure bromide composition. This demonstrated that elevated temperature and an inert atmosphere were not prerequisites for high-quality $CsPbX_3$ nanocrystals. However, these NCs were not coated as thin-films, presumably because the low reaction yield resulted in a low NC concentration which was not viable for thin-film deposition and subsequent electronic device fabrication.

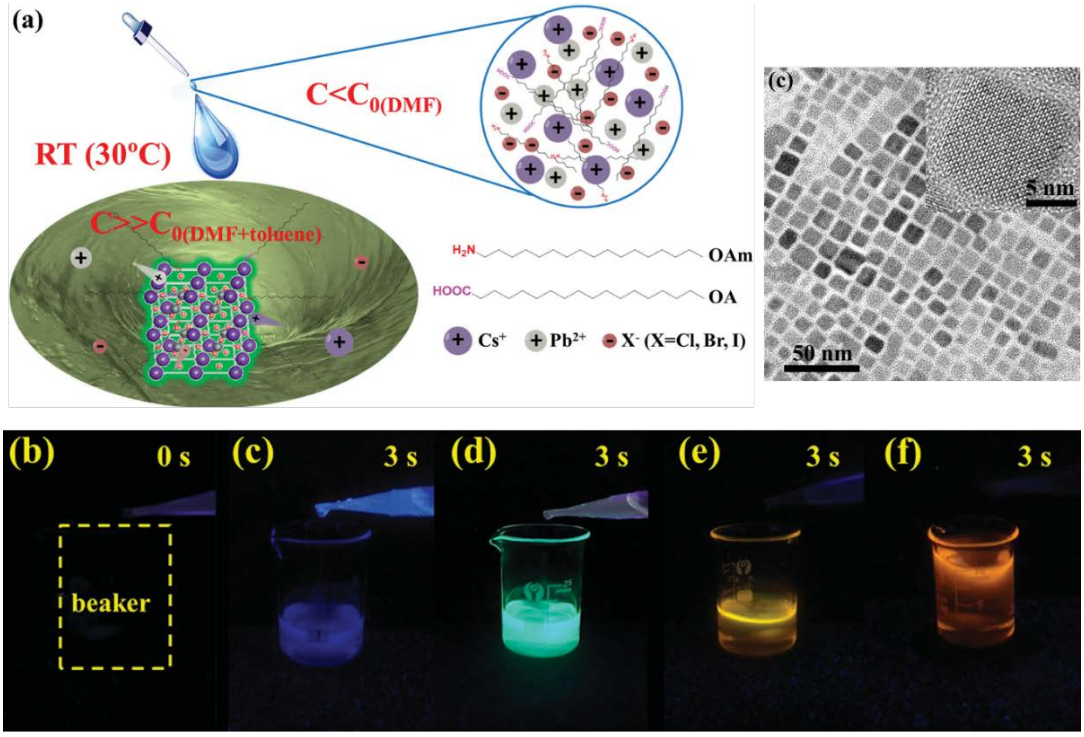

Figure 2. The first room temperature synthesis of $CsPbX_3$ nanocrystals: (a) a schematic illustrating the crystallization induced by super-saturation and showing the starting materials used, (b) $CsPbX_3$ NC solutions 3 seconds after nucleation with halide ratios of Cl:Br = 1:1, pure Br, I:Br = 1:1 and I:Br = 3:2, from left to right, and (c) TEM image of pure $CsPbBr_3$ NCs with the corresponding HRTEM in the inset. Adapted with permission from Ref.[63] Copyright 2016 John Wiley and Sons.

Veldhuis et al. pinpointed the low solubility of CsBr in DMF as a factor limiting the reaction yield of LARP.[64] To address this, they employed a crown ether to bind to Cs^+, facilitating better solubility. The cavity size of the crown ether determines the size of ion that it will selectively bind to,[65] thus dibenzo-21-crown-[7] (cavity size = 3.4 - 4.3 Å) was chosen to match Cs^+ (ionic radius = 3.3 Å). Using oleic acid and octylamine ligands, a $CsPbBr_3$ NC solution was obtained, from which the NCs could be precipitated by centrifugation. The mechanism proposed for NC formation is shown in Figure 3. Redispersion of this precipitate in fresh toluene provided a $CsPbBr_3$ NC ink from which continuous NC thin-films could be deposited. This enabled the fabrication of NC-based LEDs, leading to a modest external quantum efficiency (EQE) of 2.64 %. It is important to note that this efficiency was achieved by coating two NC films successively, with the LED fabricated from a single coating giving a lower EQE of 1.27 %. This implied that the NC ink concentration remained below the ideal concentration. However, as the volume of toluene in which the NC precipitate was redispersed was controlled, the solubility limitation here must lie with the ligands, and their ability to stabilize the dispersed phase at higher concentration.

Moyen et al. took a different approach to improving the yield of $CsPbBr_3$ NC syntheses.[66] They separated the ligands into different precursor solutions (oleylamine in DMF and oleic acid in toluene) to

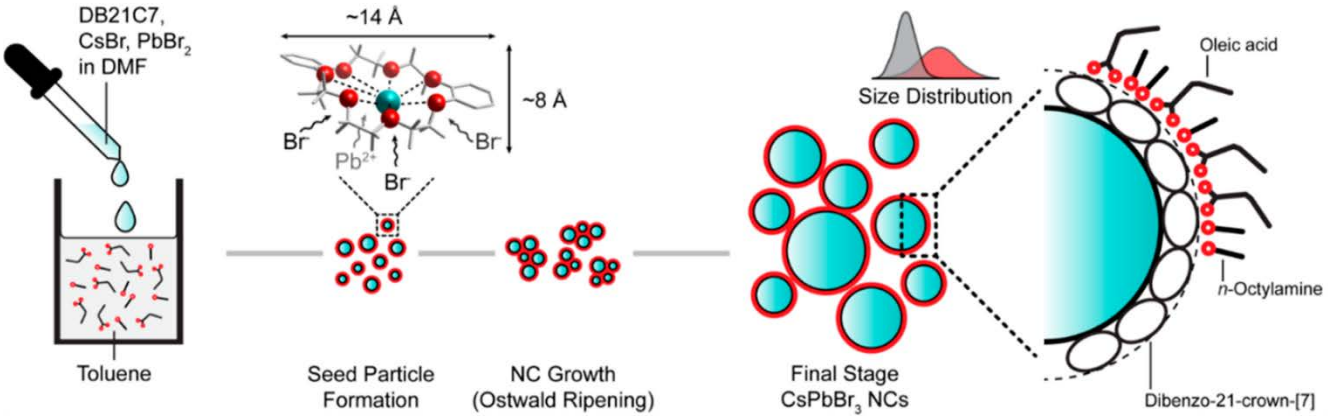

Figure 3. The proposed mechanism of the crown ether mediated synthesis of $CsPbBr_3$ NCs at room temperature. Reproduced with permission from Ref.[64] Copyright 2018 American Chemical Society.

obtain greater control over the ratio between the two ligands on the NC surface. As a result, the reaction yield was increased by ~300 %. In addition to this synthetic modification, they developed a ligand removal protocol. They first expelled large particles by centrifugation, before adding methyl acetate as an antisolvent to precipitate the NCs, removing by-products and presumably some proportion of surface ligand. After redispersing the NCs and depositing a thin-film, they reduced the surface ligand density further, and concurrently increased the NC size, by annealing at 120 °C. The removal of excess insulating ligand material is considered key to improving charge transport in a NC film. The increase of NC size is also likely to be helpful, as it would increase the proportion of intracrystal charge diffusion through the film, relative to much slower intercrystal diffusion. Accordingly, a 13-fold EQE enhancement was observed for LEDs fabricated from annealed films. Furthermore, exposing the annealed films to UV light increased the EQE a further 2.8 times. This was attributed to surface passivation by either light-assisted water adsorption or photo-oxidation.

Annealing and UV exposure are certainly industrially applicable processes. In general, post-deposition ligand removal is a useful feature as the NC ink could conceivably be distributed containing high concentrations of ligand to ensure stability, without the need for any further wet chemistry to purify before deposition. However, this approach may not be the most conducive to thin-film stability, as there is a thin line between passivation and degradation by oxidative species, particularly as the perovskite lattice is highly ionic.

The same group expanded their approach soon after, introducing a ligand exchange protocol with didodecyldimethylammonium bromide (DDAB).[67] They demonstrated that DDAB ligands were more resistant to antisolvent washing and annealing, such that oleic acid and oleylamine are mostly removed, while DDAB mostly remained. This hypothesis is illustrated in Figure 4. The effective replacement of the long oleyl ligands with DDAB led to a 10 times improvement in LED efficiency. Interestingly, the

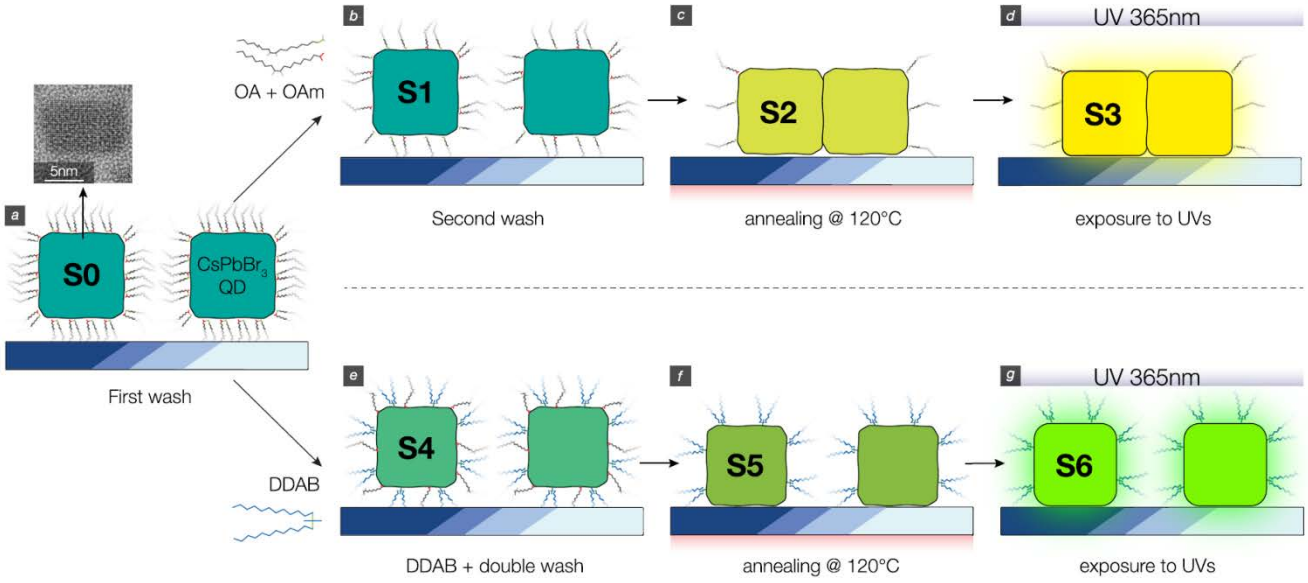

Figure 4. A schematic of the post-treatment of $CsPbBr_3$ NCs synthesized at room temperature. (a) designates the as-synthesized NCs washed once by methyl acetate, (b)-(d) represents the post- treatment process of further washing, annealing and UV exposure, and (e)-(g) represents the same post-treatment process after ligand exchange with DDAB. Reproduced with permission from Ref.[67] Copyright 2018 American Chemical Society.

efficiency increased by a further 25 % when a higher concentration NC ink was spin-coated at a higher speed. This was attributed to a more uniform film of similar thickness. It has previously been observed for chalcogenide quantum dots that smoother and more compact films have higher LED efficiency as current leakage is minimized.[68]

To circumvent the issues related to long ligands entirely, Akkerman and coworkers utilized very short ligands, propionic acid and butylamine, to synthesize $CsPbBr_3$ NCs.[69] These NCs formed large aggregated clusters but maintained confined domains of 15-20 nm, and therefore a PLQY of 58 % was obtained, similar to that achieved with longer ligands. A turbid suspension of these NCs could be spin-coated or drop-cast, with only 10 mins of drying at ambient conditions required due to the low boiling point ligands and solvents used. The lack of potentially lengthy purification or treatment steps is very appealing and would significantly reduce solvent wastage. However, it is important to note that whilst conducted at room temperature, this synthesis was performed inside a nitrogen-filled glovebox. Solar cells were fabricated from these NCs, by depositing multiple layers of NCs to obtain a film of suitable thickness (around 1 µm) and optical density. No LEDs were reported; it is likely that depositing a uniform film of <50 nm from the turbid ink of NC clusters would have been very challenging.

Ye et al. adapted Akkerman's approach for LED applications.[70] They added carefully optimized amounts of oleic acid and oleylamine to as-synthesized $CsPbBr_3$ NCs, followed by ethyl acetate to precipitate the NCs. By redispersing the nanocrystals and repeating the cycle 4 times, they achieved

complete ligand exchange while minimizing excess oleyl ligand in the final NC ink. Ligand exchange significantly improved colloidal stability, leading to LEDs with a high EQE of 5.4 %. This impressive efficiency highlights the benefits of adding the longer ligands post-synthetically, as they do not need to be added in excess.

2.2. Polar Solvent-Free Syntheses

More recently, room temperature syntheses of $CsPbX_3$ have avoided the use of DMF entirely, through the design of polar solvent-free injection methods. A key motivation for this is the extreme susceptibility of perovskite NCs to degradation by polar solvents. Using DMF in the reaction mixture, it is likely that there will be some degradation or aggregation prior to removing DMF by centrifugation. Polar solvent-free syntheses tend to employ chemistry very close to that of hot-injection syntheses, where only non-polar, non-coordinating solvents are used.

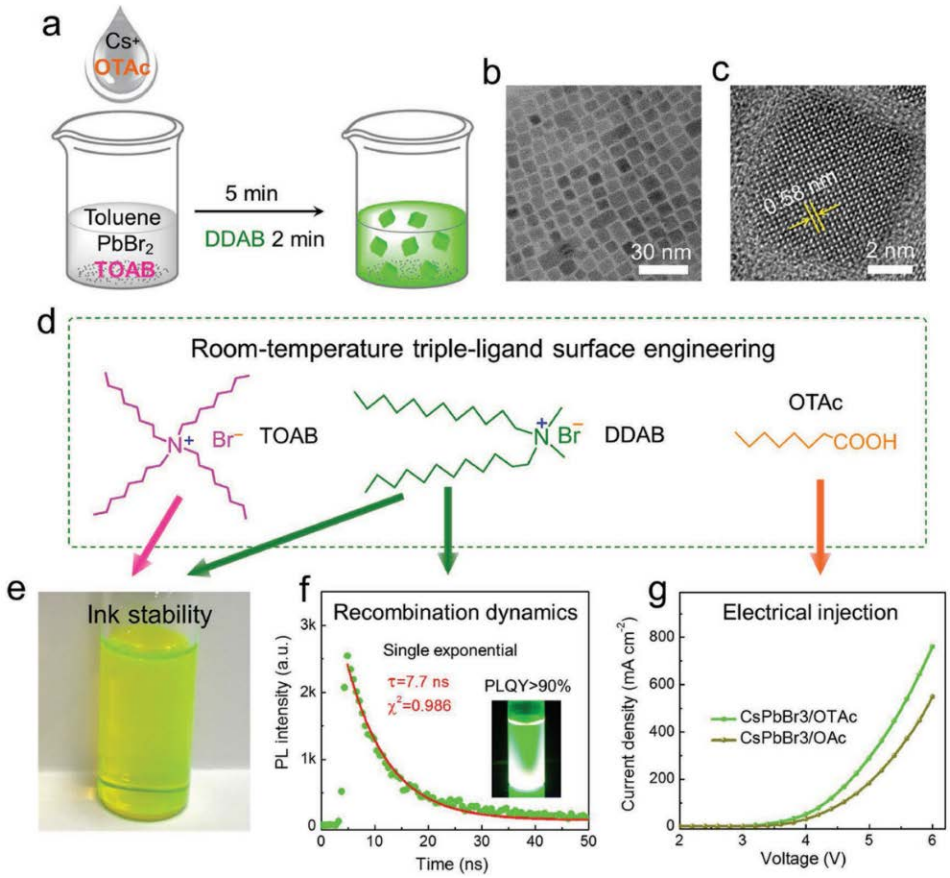

Figure 5. "Triple-ligand" surface passivation approach for $CsPbBr_3$nanocrystals: (a) The precursors and synthesis protocol, (b) TEM image, (c) HRTEM image, (d) the three ligands employed, TOAB acts only as a solvation agent while DDAB and OTAc coordinate to the NC surface, (e) photograph of the purified NC ink, (f) time-resolved photoluminescence data and (g) current density against voltage plot for LEDs fabricated from NCs with either oleic acid or octanoic acid ligands. Reproduced with permission from Ref.[41] Copyright 2018 John Wiley and Sons.

The first polar solvent-free synthesis of $CsPbBr_3$ NCs was reported by Wei et al. in 2017.[47] Analogous to the hot-injection synthesis, they separated the cesium, and lead and bromide ions into different precursors. Cesium oleate was dissolved in toluene with oleic acid at room temperature, while $PbBr_2$ was dissolved in toluene with the aid of tetraoctylammonium bromide (TOAB). TOAB can solvate $PbBr_2$ through the formation of the complex $(C_8H_{17})_4N^+Pb[Br_3]^-$. Injection of the cesium precursor into the lead bromide precursor immediately nucleated $CsPbBr_3$ NCs. It was explained that an advantage of using toluene instead of DMF was the lack of aggregated or very large NCs. These large NCs cannot be colloidally stabilized, so they are expelled by centrifugation, severely reducing the reaction yield. With toluene as the only solvent, they obtained $CsPbBr_3$ NCs with PLQY > 80 %. Furthermore, they demonstrated the scalability of their approach by conducting a 1 L scale synthesis, a 40 times scale-up, achieving comparable PLQY. Despite this, the EQE obtained from LEDs using these NCs was very low (0.015 %).

Song et al. sought to improve the suitability of this polar solvent-free synthesis for LED applications by utilizing shorter ligands (Figure 5).[41] Firstly, the oily oleic acid ligand was replaced by octanoic acid, in which Cs_2CO_3 can be dissolved directly at room temperature. Secondly, in addition to TOAB, DDAB was added to the crude solution 5 minutes after nucleation. The nitrogen content before and after DDAB treatment was studied by XPS, proving that only DDAB and octanoic acid act as ligands on the NC surface. TOAB acts only as a solvation agent, as the large steric hindrance of its 4 octyl groups prevent binding to the surface.

2.3. Antisolvent Purification

Effective antisolvent purification is essential to ensure that NC inks are free from reaction by-products and excesses. A commercial NC ink must be highly reproducible with minimal impurities. For electronic device applications, removal of excess ligand material is crucial. This is because these ligands are usually organic and very poor conductors. Therefore, excess ligand will impede current flow and reduce device performance, and not necessarily in a consistent manner. Furthermore, often the ligands employed are viscous and oily, such that the physical properties of the solution and thin-film may be altered if they are present in excess.

There have been a few reports focused on identifying suitable antisolvents. A general consensus is that the solvent must be aprotic, as protic solvents can promote the extraction of lead ions from the nanocrystal.[43–45] The solvent must also be of medium polarity; that is, polar enough to precipitate the NCs easily, but not so polar as to remove bound ligands or degrade the perovskite crystal during short-term exposure. Typically, short esters have been most successful. Depending on the ligand system employed, butyl acetate,[44] ethyl acetate,[35,41,43,71–77] mixtures of ethyl and methyl acetate,[78,79] and methyl acetate alone,[67,80–83] have been employed. Figure 6 shows a screening study of 36 potential

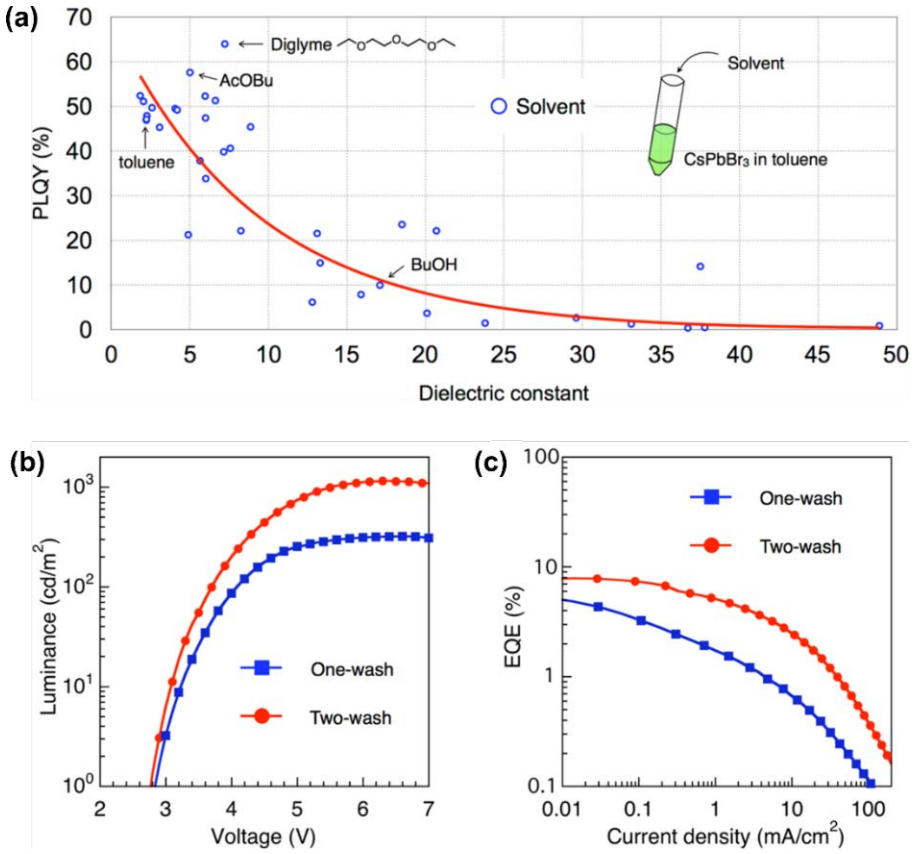

Figure 6. The impact of antisolvent purification on perovskite NC properties: (a) plot of $CsPbBr_3$ NC PLQY against dielectric constant for 36 different antisolvents, and (b) and (c) the improvement of LED luminance and EQE, respectively, after an additional antisolvent washing cycle with diglyme. Adapted with permission from Ref.[45] Copyright 2018 American Chemical Society.

antisolvents, it concurred on the efficacy of short esters, but indicated that diethylene glycol dimethyl ether (diglyme) was the most effective.[45] They subsequently demonstrated that purifying $CsPbBr_3$ NCs with diglyme instead of methyl acetate yielded higher LED efficiency.

Clearly, strongly bound ligands are highly desirable for complete purification, as they allow the NCs to be fully precipitated, thus minimizing mass loss, without the risk of minor degradation or ligand removal, which would limit the reproducibility of purification. Furthermore, it is reasonable to assume that an antisolvent with higher polarity (or higher dielectric constant) will remove impurities more effectively, thus NCs which can withstand more polar solvents should be more thoroughly purified. This point is well-illustrated by the octylphosphonic acid ligands utilized by Tan et al. They demonstrated that with these strongly bound ligands, the NCs could withstand 8 purification cycles with methyl acetate without significant loss of PLQY (Figure 7).[80] This remarkable stability towards antisolvent washing was later attributed to the inter-ligand hydrogen bonding between adjacent octylphosphonate ligands.[73]

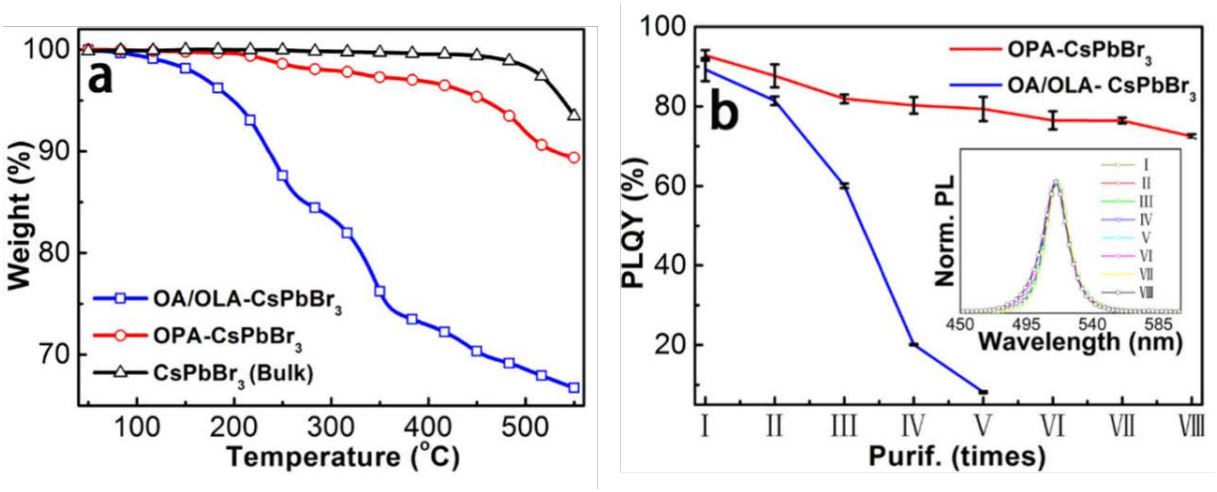

Figure 7. A comparison of strong binding octylphosphonic acid (OPA) ligands with the oleic acid/oleylamine (OA/OLA) ligand system: (a) thermogravimetric analysis, showing the weight percentage corresponding to organic material (i.e. ligands) and (b) the change in PLQY of OPA and OA/OLA-capped $CsPbBr_3$ NCs with multiple methyl acetate purification cycles (inset shows PL curves for all OPA samples). Adapted with permission from Ref.[80] Copyright 2018 American Chemical Society.

3. Ligand Engineering

3.1. Beyond Dynamic Ligand Binding

The drive to replace amine ligands was primarily based on stability concerns, as amine-capped nanocrystals would readily precipitate from solution. This was attributed to the highly dynamic binding of the acid/base pair, such that rapid proton transfer between the amine/ammonium and carboxylic acid/carboxylate occurred.[84] As a result, the ligands are prone to desorption from the NC surface. New ligands have been sought that bind more strongly and, crucially, irreversibly to perovskite NC surfaces. A wide range of alternative ligands have been explored, most often using high temperature syntheses. However, it is probable that most, if not all, of these ligands could be simply applied in room temperature syntheses, utilizing solubilizing agents if necessary.

3.2. Quaternary Ammonium Halides

Quaternary ammonium halides have become a ubiquitous ligands for $CsPbBr_3$ NCs,[37,41,44,67,72,85–87] representing an upgrade on the initial amine ligands. Quaternary ammonium halides contain the same binding functionality that a primary amine provides, but are unable to participate in proton exchange. DDAB is particularly appealing as it provides better colloidal stability from shorter alkyl chains. It contains two C_{12} alkyl chains, presenting greater steric bulk. Recently, a study by Park et al. compared $CsPbBr_3$ NCs capped with quaternary ammonium bromide ligands with 1, 2, 3 or 4 long-chain groups

attached to the N^+ center.[40] They confirmed that 2 long chains (with the other 2 being methyls) provided the highest EQE in LEDs, but also that using the slightly shorter decyl groups enhanced EQE relative to the dodecyl groups on DDAB.

It is likely that the ability of DDAB to interrupt interparticle ligand-ligand interdigitation is also key to the colloidal stability it affords. The interdigitation of straight chain ligands on adjacent particles has been correlated to lower solubility, due to the high enthalpic cost of untangling the chains.[34] The "triple ligand" approach mentioned earlier, where TOAB solubilized $PbBr_2$, Cs_2CO_3 was dissolved in octanoic acid, and DDAB passivated the NC surface, has enabled $CsPbBr_3$ NC LEDs with up to 6 % EQE.[41] This efficiency was partly attributable to the substitution of oleic acid for octanoic acid; NCs synthesized with octanoic acid showed higher electron and hole currents in single carrier devices, indicating improved electron injection and conductivity in the film. Generally, higher currents can also be attributed to a lower quantity of excess unbound ligand or other insulating synthetic by-products in the film. The greater colloidal stability provided by DDAB allowed high-quality, highly concentrated NC inks to maintain their properties through two antisolvent washing cycles with ethyl acetate.

In order to push the EQE of their NC LEDs higher, Song et. al. employed a simple FA doping strategy. By dissolving formamidine acetate in octanoic acid alongside Cs_2CO_3, $Cs_{1-x}FA_xPbBr_3$ NCs were obtained. This resulted in a dramatic improvement to 11.6 % EQE with an optimum value of $x = 0.15$, which was supported by time-resolved photoluminescence (TRPL) showing a doubling of the radiative recombination lifetime (τ_2).

3.3. Metal Halides

Song et al. developed their triple ligand $Cs_{1-x}FA_xPbBr_3$ NC synthesis further by including a second post-nucleation treatment after DDAB. They introduced a metal bromide solution (MBr_x, M = Zn^{2+}, Mn^{2+}, Ga^{3+} or In^{3+}), dissolved in toluene with TOAB, after a further 3 minutes.[37] The metal bromides acted only as passivating agents; XPS showed a 3 times reduction in octanoic acid content, alongside an increase in the Br:Pb ratio, suggesting the metal bromides substituted for octanoic acid on the NC surface, as illustrated in Figure 8. This further reduction in surface ligand density on the NCs was correlated to the resulting record EQE of 16.48 % obtained from LEDs. This was accompanied by an increase in operational stability from 37 mins to 136 mins. Despite NC solutions with and without MBr_x passivation showing solution PLQYs > 90 %, it was found that after MBr_x passivation, the retention of PLQY from solution to thin-film was much better. This highlights the importance of reporting thin-film PLQY, not only solution PLQY, when correlating NC properties to LED performance.

It is not clear exactly which factors govern the degree of PLQY drop from solution to film. Although managing the morphology of perovskite NC films is much less complicated than controlling the crystal growth of quasi-2D or 3D perovskite during coating, the uniformity of films remains important. A study

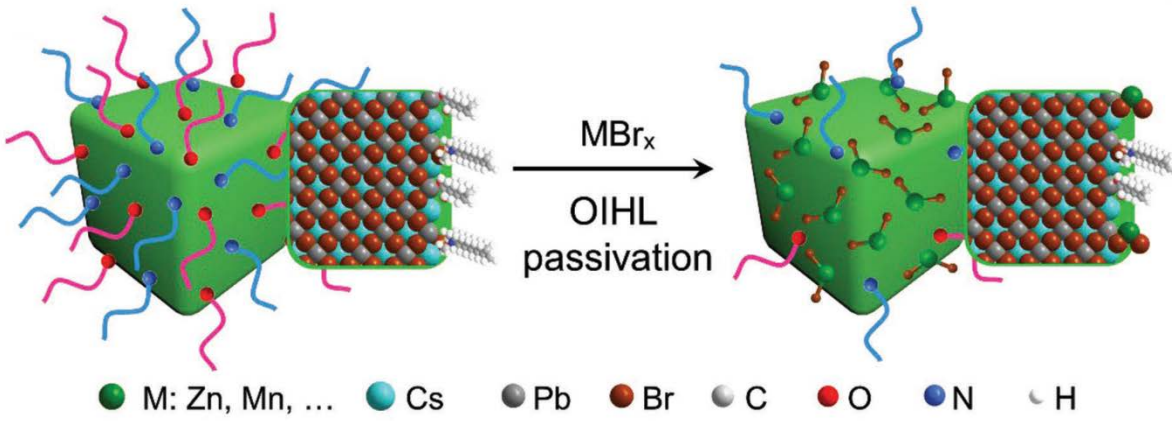

Figure 8. A schematic of the metal bromide passivation treatment of $Cs_{0.85}FA_{0.15}PbBr_3$ NCs, illustrating the substitution of octanoic acid for metal bromides. Reproduced with permission from Ref.[37] Copyright 2018 John Wiley and Sons.

on CdSe/ZnS quantum dots has shown that spin-coating nanoparticle films from a highly volatile solvent (hexane) yields rougher films than a less volatile solvent (octane) as strong capillary forces from rapid evaporation induce film thickness fluctuations.[68] This resulted in poorer charge injection efficiency in LEDs and ~40 % lower EQE.

3.4. Anionic Ligands

In contrast to quaternary ammonium halides, where the ammonium binds strongly to anionic sites while the halide binds to under-coordinated lead sites (i.e. halide vacancies), there have been several recent reports where anionic surface ligands are used to passivate these positively charged sites. While these ligands have so far mostly been utilized for hot-injection syntheses, their solubility in non-polar solvents, alone or with assistance from co-ligands such as TOAB[41,47,75] or trioctylphosphine oxide (TOPO),[80,88] implies that they should be compatible with established room temperature syntheses.

Previously, we discussed the common use of simple carboxylic acids, such as oleic and octanoic acid, and their generally weak binding to perovskite nanocrystals. Nenon et al. correlated this to a hard-soft mismatch between the ligand binding group and the lead ions;[38] that is, the electron density on the carboxylic acid group is too high to interact sufficiently strongly with the large, diffuse charge on Pb^{2+}. Consequently, they showed that ligand substituents which withdraw electron density from the carboxylic acid group, such as aromatic or fluorinated aliphatic groups, facilitate stronger ligand binding. This theory is summarized by the depiction of a $CsPbX_3$ NC surface in Figure 9. Softer acid groups, such as phosphonic and sulfonic acids, were found to bind similarly strongly, further evidencing this theory.

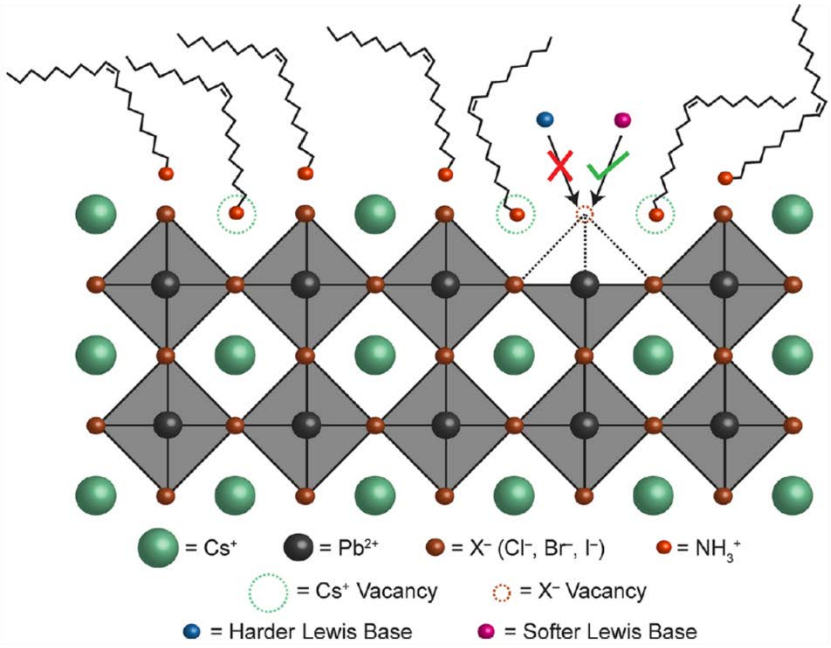

Figure 9. Depiction of a typical $CsPbX_3$ NC surface, showing that ligands which are softer Lewis bases can bind to halide vacancies, whereas harder Lewis bases (such as aliphatic carboxylic acids) cannot. Reproduced with permission from Ref.[38] Copyright 2018 American Chemical Society.

Pan et al. utilized a softer, bidentate carboxylic acid, 2,2-iminodibenzoic acid (IDA), as a post-synthetic ligand treatment for $CsPbI_3$ NCs.[71] They noted that their attempt to incorporate IDA in the synthesis led to NC agglomeration, presumably because it is too short to provide sufficient colloidal stability. They instead simply added IDA powder to the $CsPbI_3$ NC solution after a standard hot-injection synthesis.

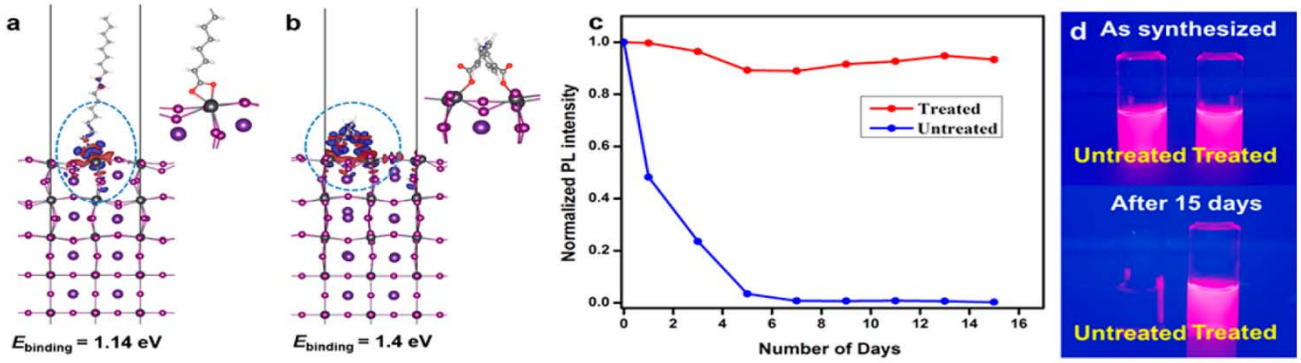

Figure 10. The effect of the bidentate 2,2'-iminodibenzoic acid (IDA) ligands on $CsPbI_3$ NCs compared to oleic acid (OA): (a) and (b) the results of density functional theory calculations for the binding of OA and IDA, respectively, to the NC surface, (c) the change in PL intensity over time with and without IDA treatment, and (d) photographs taken of $CsPbI_3$ under UV light, with and without IDA treatment, fresh and after 15 days. Reproduced with permission from Ref.[71] (https://pubs.acs.org/doi/10.1021/jacs.7b10647). Further permissions related to the material excerpted should be directed to ACS.

IDA stabilized the NCs effectively, enabling retention of PLQY for over 15 days (Figure 10), in stark contrast to the untreated NCs whose PLQY was completely quenched after 7 days. In the case of $CsPbI_3$, this was presumably due to conversion to the thermodynamically favored, non-emissive phase upon aggregation. It is conceivable that short bidentate ligands such as IDA could be incorporated into room temperature syntheses with appropriate solubilizing agents, however a longer chain co-ligand would be required to ensure colloidal stability.

3.4.1. Phosphonic Acids

As well as softer carboxylic acids, there have been a few reports of $CsPbBr_3$ NCs synthesized using phosphonic acid ligands. As mentioned earlier, the replacement of oleic acid and oleylamine with octylphosphonic acid (OPA) improved antisolvent tolerance remarkably.[80] In order to solubilize OPA in the reaction mixture, TOPO was added. TOPO can help to solubilize phosphonic acids through hydrogen bonding interactions. This approach should also be effective for solubilizing other acids in non-polar solvents. The presence of two hydroxyl and one phosphonyl group on the same binding head allows phosphonic acids to bind to a surface with an anionic group (i.e. P-O^-) while retaining the capacity to form two hydrogen bonds (see Figure 11b for diagram).[73] This is a unique property of phosphonic acids, which enables the formation of inter-ligand hydrogen bonds to enhance NC binding. However,

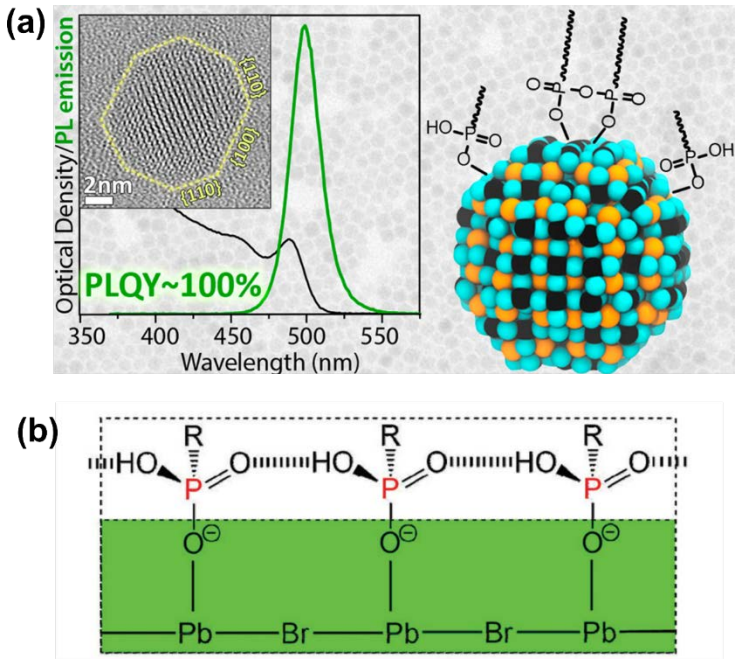

Figure 11. The use of phosphonic acid ligands for $CsPbBr_3$ NC passivation: (a) phosphonic acids and phosphonic acid anhydrides facilitated near-unity PLQY, absorbance and PL spectra are shown with HRTEM image in the inset and TEM image in background (adapted with permission from Ref.[76] Copyright 2019 American Chemical Society), and (b) the proposed inter-ligand hydrogen bonding motif formed between adjacent octylphosphonate species on the NC surface (adapted with permission from Ref.[73] Copyright 2019 Royal Society of Chemistry).

similar surface chemistry could be envisaged for sulfonic acid groups binding to a surface as a Lewis base through a sulfonyl group. Though a Lewis Base-type interaction is unlikely to be as strong, and sulfonic acids would instead be expected to bind to the ionic perovskite surface through the S-O^- of a sulfonate group.

Further interesting binding chemistry with phosphonic acids was reported by Zhang et al.[76] They discovered that the conditions of the hot-injection method drove a condensation reaction, forming phosphonic acid anhydrides from phosphonic acids. These phosphonic acid anhydride species could then form bidentate bonds to the $CsPbBr_3$ NC surface (Figure 11a), presumably because the distance between adjacent hydroxyl groups on the anhydride was similar to the spacing between lead sites of the NC. Thus, the introduction of phosphonic acid anhydrides to room temperature syntheses provides an alternative passivation strategy to explore, where the bidentate anchoring may improve NC stability. However, Zhang and co-workers pointed out that while the colloidal stability with these phosphonic acid ligands was high, they were prone to desorption when the dispersion was heated to 50 °C. An investigation is required into whether this thermal instability is also observed for thin films of NCs. It would represent a serious problem for utilizing phosphonic acid capped perovskite NCs in electronic devices, where Joule heating can be expected to raise the local operating temperature.[89]

3.4.2. Sulfonic Acids

Sulfonic acids have also been explored using the hot-injection approach. Yang et al. employed solely dodecylbenzene sulfonic acid (DBSA) as the ligand to cap $CsPbBr_3$ NCs.[90] Electron density simulations, shown in Figure 12a, indicated that the sulfonate group can effectively passivate bromide vacancies on the surface of $CsPbBr_3$ NCs. Similar to phosphonic acids, DBSA proved strongly resistant to antisolvent purification, with surface ligand density, and consequently PLQY, mostly retained over 8 cycles. Furthermore, long-term stability testing was undertaken, demonstrating the DBSA-capped NCs retained colloidal stability and PLQY over 5 months in air (Figures 12b and 12c). This is a very relevant test for commercial purposes, where an extensive shelf life is a prerequisite. They also investigated thermal stability, by annealing NC films for 1 week at 60 °C. The PL peak position was maintained over this period and there was only a 10 % drop in PL intensity, which suggests that sulfonic acid ligands may exhibit more thermally robust binding with $CsPbBr_3$ NCs than phosphonic acids.

There has been one other report which utilized the sulfonate binding group. Ye et al. investigated a post-synthetic treatment of $CsPbBr_{1.5}Cl_{1.5}$ NCs with two different sulfonate salts: tetrabutylammonium p-toluenesulfonate (TBSA) and sodium dodecylbenzenesulfonate (SDSA).[91] TBSA induced a significant blueshift of the PL emission wavelength while SDSA induced a redshift, essentially to a wavelength corresponding to $CsPbBr_3$ emission. The anion exchange was found to depend of both the cation and anion of the salt but the mechanism was not fully elucidated. Nevertheless, all treated samples exhibited

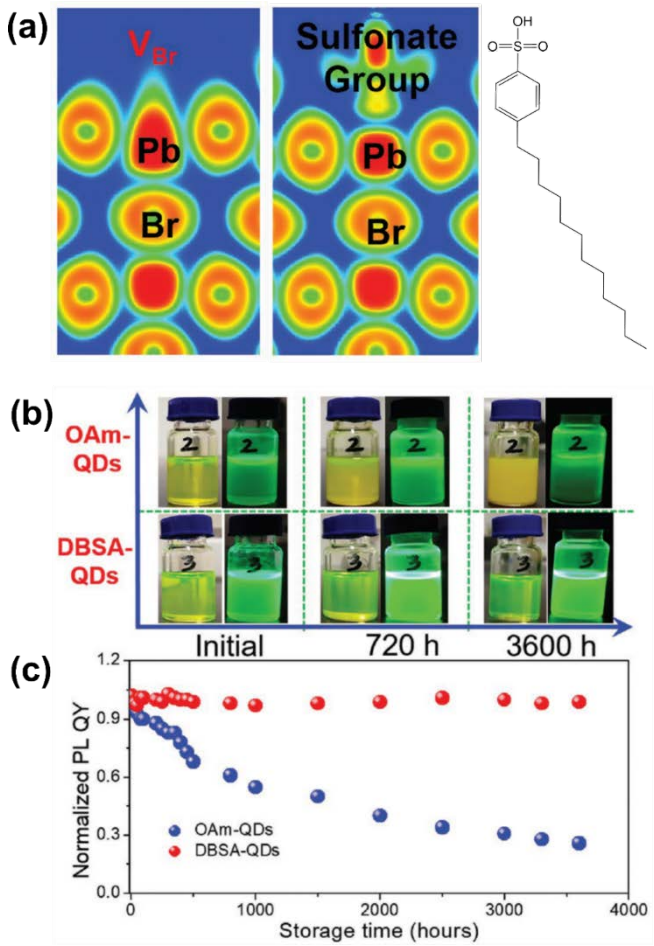

Figure 12. Dodecylbenzene sulfonic acid (DBSA) as a ligand for $CsPbBr_3$ NCs: (a) electron density simulations showing the passivation of a bromide vacancy by a sulfonate group, (b) photographs of oleylamine (OLA) and DBSA-capped NCs under both visible and UV light after different storage times, and (c) the change in PLQY of OLA and DBSA-capped NCs over long-term storage (3600 hours). Adapted with permission from Ref.[90]. Copyright 2019 John Wiley and Sons.

enhanced PLQY, which was attributed to the strong binding sulfonate ligand head groups. The use of salts to release anionic ligands here is an interesting approach. Given that tetraoctylammonium bromide has been frequently used to facilitate polar solvent-free room temperature perovskite NC syntheses, it is likely that quaternary ammonium sulfonate or phosphonate salts could be directly employed in the NC synthesis for strong passivation without the need for post-synthetic exchange.

3.5. Zwitterionic Ligands

A distinctly different ligand engineering approach was taken by Krieg et al. Rather than combining anionic or cationic species as co-ligands, they exploited zwitterionic ligands, which are dipolar molecules with two charged functional groups: one positively charged and one negatively.[92] These bind in a bidentate manner, coordinating to a cationic and anionic surface sites simultaneously, thus affording additional stability according to the chelate effect. Three different types of zwitterion were tested with

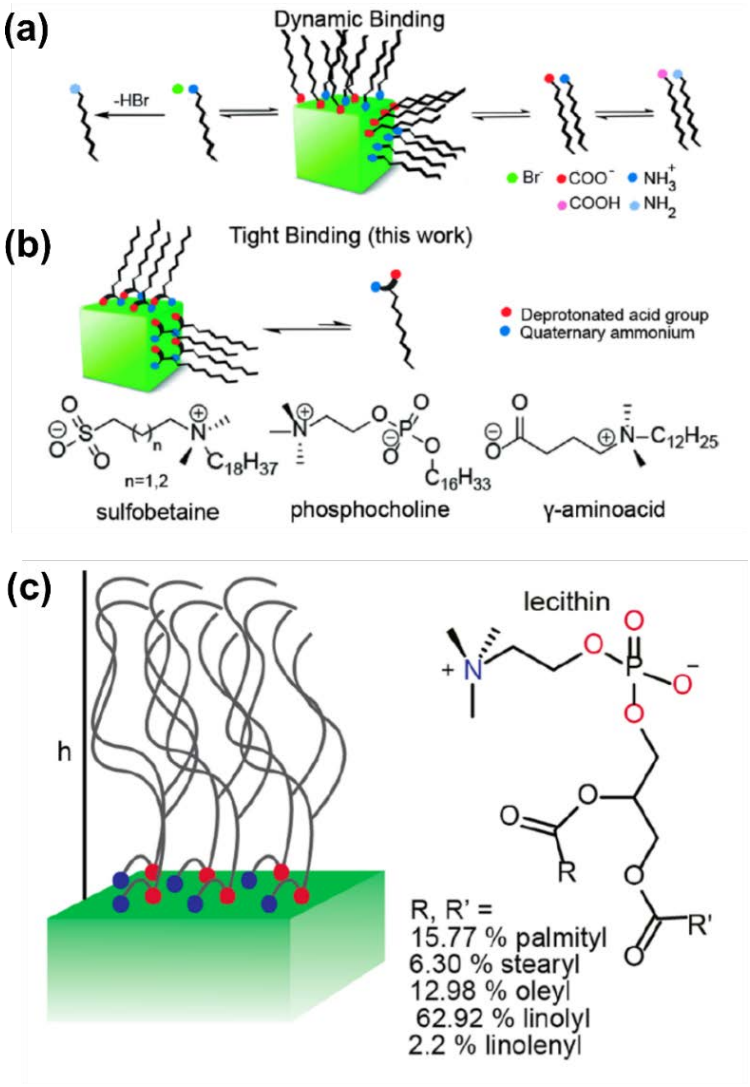

Figure 13. Zwitterionic ligands: (a) the weak dynamic binding of typical carboxylic acid/amine ligands, (b) the tight binding of zwitterionic ligands and structures of 3 such ligands that were tested, and (c) the binding and structure of soy lecithin. Adapted with with permission from Refs[92,94] (https://pubs.acs.org/doi/10.1021/acsenergylett.8b00035 and https://pubs.acs.org/doi/10.1021/jacs.9b09969) Further permissions related to the material excerpted should be directed to ACS.

$CsPbBr_3$ NCs, all of which had quaternary ammonium groups but different anionic groups. These included a sulfobetaine (3-(N,N-dimethyloctadecylammonio)-propanesulfonate), which contains a sulfonate group, a phosphocholine (N-hexadecylphosphocholine), which contains a phosphate group, and a γ-amino acid (N,N-dimethyldodecylammoniumbutyrate), which contains a carboxylate group. Figure 13 shows the structures of each of these ligands, alongside schematics comparing their tight binding to the dynamic binding of the carboxylic acid/amine system. The sulfobetaine was studied in more detail; they found that by adjusting the length of the alkyl spacer, thus changing the gap between the functional groups, the ligand could be tailored for chloride, bromide and iodide NCs, which have different lattice parameters. The sulfobetaine exhibited is particularly attractive commercially as it is a

ubiquitous low-cost detergent. Later, Ochsenbein et al. demonstrated that this long-chain sulfobetaine does not severely inhibit inter-nanocrystal conductivity, by fabricating blue-emitting LEDs from $CsPb(Br/Cl)_3$ NCs, yielding an impressive EQE for blue emission of 1.4 %.[93]

These zwitterionic ligands enable far more concentrated colloidal inks than typical ligands, which broadens the range of potential applications. The same group took this a step further recently, utilizing soy lecithin as a ligand - a low-cost, mass-produced, zwitterionic phospholipid.[94] Soy lecithin contains a long polydisperse branched alkyl chain (see Figure 13), thus as discussed earlier, there will be little enthalpic driving force to pack the ligand chains together and a huge entropic barrier.[34,42] With this ligand, $CsPbBr_3$ NC inks with concentration ranging from ng/mL to > 400 mg/mL were obtained; as a result, both isolated single NCs and thin-films with thicknesses up to 1.5 µm were feasible. Although charge transport through NC films with such a large insulting ligand would be greatly hindered, it does afford great versatility for non-conducting applications.

4. Future Directions

4.1. Novel Ligands

4.1.1. Entropic Ligands

As mentioned earlier, the improved colloidal stability with DDAB ligands can be correlated to the presence of multiple long alkyl chains attached to a single binding group. This inhibits the interdigitation of alkyl chains, making NC aggregation less favorable. It is possible to further exploit this effect. It has been demonstrated that CdSe quantum dots were over 100 times more soluble with branched chain ligands than straight chain, as shown in Figure 14.[42] As well as reducing the enthalpic cost of dissolution, branched chains increased the entropy released due to a greater number of intramolecular

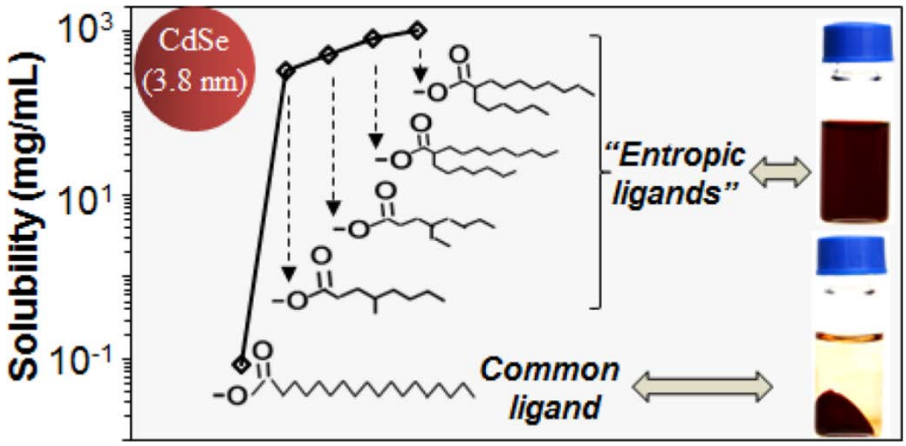

Figure 14. The impact of ligand branching on the solubility of CdSe quantum dots. Reproduced with permission from Ref.[42] Copyright American Chemical Society 2016.

bond rotation and bending freedoms. Thus, highly stable NC inks of high concentration should be attainable with short branched-chain ligands, which would minimize the contribution of ligands to resistivity in NC thin-films. This is in agreement with the enormous increase in colloidal stability obtained with very long, highly branched, soy lecithin,[94]. However, this concept has not yet been explored for shorter chain ligands suitable for perovskite NC LEDs. There are many commercially available branched-chain carboxylic acids and amines, as well as recent reported syntheses of branched phosphonic acids.[95]

4.1.2. Polymerizable Ligands

The highly ionic nature of the perovskite lattice inevitably means that any nanocrystal surfaces remain prone to degradation by polar species even when capped by organic ligands. One approach to provide more robust protection to perovskite NCs has been to mix with polymer, thus enabling highly stable composite films.[96] Another option is synthesizing core-shell structures with a stable material such as SiO_2.[97] However, while useful for optically-driven applications, these routes are unsuitable for electrically-driven applications such as LEDs, where large domains of insulting material severely inhibit charge transport.

Ideally, a thin, dense polymer shell would be employed, such that the shell contributes no more to the resistivity of the film than typical organic ligands. Polymerizable ligands may offer a route towards this, as cross-linking between chains would increase ligand shell coverage without increasing the distance between nanocrystals. Sun et al. investigated this approach, synthesizing a quaternary ammonium chloride salt containing a vinyl group, 4-vinylbenzyldimethyloctadecylammonium chloride, and using it

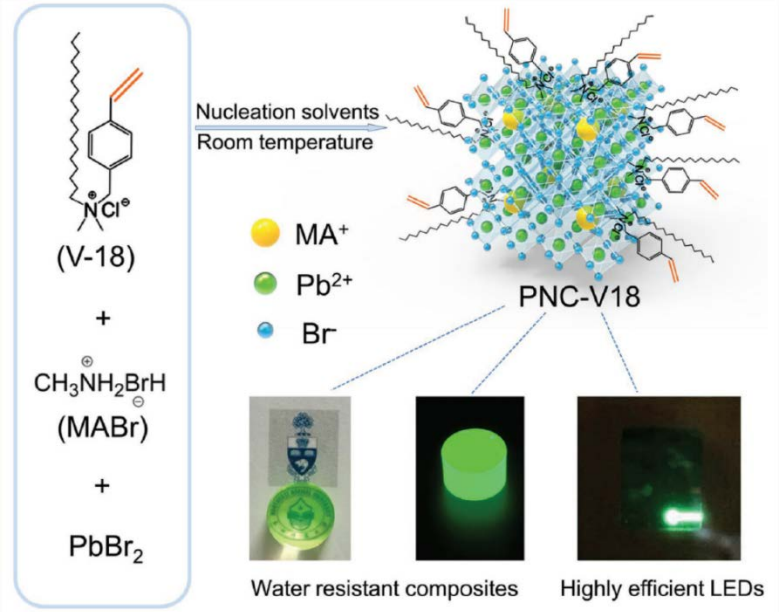

Figure 15. 4-vinylbenzyldimethyloctadecylammonium chloride as a polymerizable ligand for $MAPbBr_3$ nanocrystals. Reproduced with permission from Ref.[98]. Copyright 2017 John Wiley and Sons.

as a ligand for LARP-synthesized $MAPbBr_3$ NCs (Figure 15).[98] By adding the initiator azobisisobutyronitrile (AIBN) into the NC ink and heating the subsequently deposited NC film at 90 °C, ligand cross-linking was achieved. The stability of the film with respect to moisture was improved slightly and LEDs were fabricated successfully with a maximum EQE of 0.58 %.

The above work represented a substantial first step but there has been little advancement since. Given the wide range of monomer groups available, a group could be sought which could be cross-linked without heating the temperature-sensitive perovskite, or without adding an initiator. UV cross-linking is an attractive possibility. It is also important to ensure the ligand chain is not too long, such that film conductivity is maintained, and to consider branching for good colloidal stability. Lastly, combining these properties with a strong binding head group, such as phosphonic or sulfonic acid, will ensure the ligand shell remains firmly attached to the NC surface. Clearly, designing the synthesis of such a molecule would be challenging, but it could prove crucial to upgrading the stability of perovskite NC films to a commercially acceptable level.

4.2. Compositional Engineering

4.2.1. Metal Doping

The application of crown ethers to coordinate metal ions for perovskite NC synthesis is an interesting approach. Besides obvious extensions of Veldhuis and coworkers' efforts (e.g. solubilizing other alkali metal ions such as Rb^+ or K^+ for A-site doping or passivation),[77,79,87,99–101] the selectivity of crown ether coordination may allow the direct synthesis of transition metal-doped $CsPbX_3$ NCs at room temperature by coordinating Pb^{2+}.[102] Crown ethers coordinate more strongly to metal ions with an ionic radius close to their cavity size, thus selecting the appropriate crown ether for Pb^{2+} could impede the formation of the thermodynamically favored pure $CsPbX_3$ perovskite, allowing smaller dopant metal ions to occupy some lead sites. It has been previously proposed that NC doping is often a kinetically-controlled process, such that reduction of the growth rate promotes adsorption of dopants, thus increasing dopant incorporation.[103,104] Dutta et al. showed that this concept applies to perovskite NCs, by using solvent polarity to control the release of Pb^{2+} during $CsPbCl_3$ NC synthesis. They found that lower polarity solvents slowed the reaction rate, such that Mn^{2+} doping of up to 2 % was obtained with hexane, compared to <0.01 % when chloroform was used.[105]

Transition metal doping in perovskite NCs has been achieved for many different ions using high temperature synthesis, but there have been few room temperature examples. Doping $CsPbBr_3$ with minor concentrations of smaller transition metal ions, such Ni^{2+},[106,107] Cu^{2+},[108] Zn^{2+},[109–111] Cd^{2+} [111,112] and Al^{3+},[113] can have beneficial effects such as improved thermodynamic stability and higher PLQY,[114,115] while an accompanying blue-shift offers a route to blue emitting perovskite nanocrystals without halide mixing. This is important as the high susceptibility of mixed-halide NCs to halide segregation under

electric field raises concerns about whether they could ever obtain the color stability necessary to be commercially viable for LED applications.[93,116] Mn^{2+} doping could offer an analogous route to lower bandgap emission, owing to its luminescence peak around 600 nm from a d-d transition.[117–120] The mixing of pure bromide NCs of different colors may enable electrically-driven white-emitting all-perovskite NC LEDs, as only optically benign bromide-bromide halide exchange would occur.

4.2.2. A-Site Doping

Various fundamental studies have shown that the organic cations in the perovskite lattice (MA or FA) enhance carrier lifetimes because the rotation of asymmetrical cations in the lead halide cages increases orbital overlap and promotes large polaron formation.[121–125] The implication of the aforementioned work by Song et al. is that this enhancement can be obtained when organic cations constitute only a small percentage of the lattice, as demonstrated by the time-resolved photoluminescence and LED plots in Figure 16.[41] Given that the performance of pure $CsPbBr_3$ NC LEDs currently lags behind those containing organic cations, it may be the case that FA (or MA) doping is essential in order to obtain perovskite NC-based LEDs with EQE approaching the theoretical limit. It is therefore imperative that the impact of minor FA doping on $CsPbX_3$ NCs is analyzed in more detail. It is particularly important to assess the impact on stability: colloidal, environmental and device.

It is pertinent to point out that this concept could be extended to blue emission. Given that only a small proportion of FA is required, $Cs_{1-x}FA_xPbBr_{3-y}Cl_y$ NCs may provide a route to push the EQE of deep-blue NC-based LEDs beyond 2 %.[9] Despite reports of near-unity PLQY for deep-blue emitting NCs, their efficiency in LEDs is still much lower their green emitting counterparts. The inclusion of rubidium

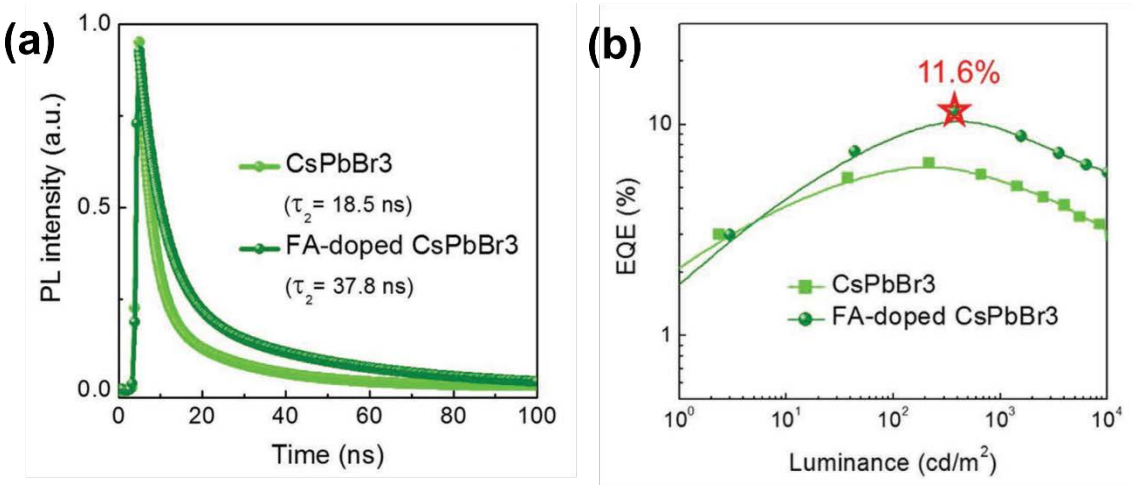

Figure 16. Comparison of pure $CsPbBr_3$ and $Cs_{0.85}FA_{0.15}PbBr_3$ nanocrystals: (a) time-resolved photoluminescence (TRPL) spectrum, and (b) external quantum efficiency against luminance plot for NC LEDs. Adapted with permission from Ref.[41]. Copyright 2018 John Wiley and Sons.

could also be employed to offset red-shifting of the emission wavelength or even circumvent the need for Cl doping,[79] perhaps in combination with transition metal B-site doping. Often as the proportion of chloride in bromide-chloride nanocrystals is increased, the PLQY and resultant EQE of LEDs decrease.[86] Therefore, blueshifting the emission wavelength without increasing the Cl:Br ratio may enable higher efficiency deep-blue emitting LEDs.

4.3. Scalable Deposition Techniques

The rapid rise of perovskite nanocrystal-based electronic devices has been almost exclusively facilitated by spin-coating. It is a simple, reproducible deposition method which can achieve good uniformity and precise thickness control for small area thin films; thus it is ideal for early-stage research. However, spin-coating prevents full access to the benefits of solution-processing. Spin-coating is a batch process, with inherently limited scalability, which operates with significant material wastage; the vast majority of ink dropped onto the substrate is ejected from the surface during coating, which is highly undesirable both from economic and sustainability perspectives.

There are various more suitable, scalable deposition techniques, which have been pioneered in organic electronics and utilized frequently for perovskite solar cell fabrication. These include slot-die coating, blade (or bar) coating, inkjet printing, and spray coating.[126,127] Applying these techniques for bulk perovskite thin film formation adds complexity. As crystallization occurs during deposition, it must be precisely controlled and expedited to obtain high quality films. The only perovskite LED so far fabricated by a scalable method was reported by Prakasam et al.; they utilized N_2 gas-assisted crystallization of $MAPbBr_3$ during slot-die coating.[128]

Perovskite nanocrystals offer a much simpler alternative; they are pre-synthesized, so crystallization and deposition processes are decoupled. There is no need for additional provisions such as N_2 gas flow or antisolvent dripping. Therefore, it seems entirely feasible that high quality perovskite nanocrystals could be easily deposited by high-throughput, roll-to-roll compatible techniques, to form high quality films for device applications. It is likely that some solvent engineering will be required so that the films dry efficiently, a process that is inherently achieved in-situ during spin-coating. The existing extensive knowledge obtained from research on scalable deposition for organic electronics provides a strong starting point. Ultimately, successful optimization of uniform, scalable perovskite NC deposition is a realistic goal which would greatly enhance commercial viability.

4.4. Lead-Free Perovskite Nanocrystals

This Progress Report has focused on lead halide perovskite nanocrystals. There are well-known toxicity concerns associated with the use of lead-containing materials in commercial optoelectronics, which

clearly weakens their industrial appeal. However, as is the case for the perovskite solar cells being pushed towards the market, and the cadmium-containing quantum dots already used in QLED displays, the poor performance of non-toxic alternatives leaves the toxic material as the only currently viable option.[129–131]

Unsurprisingly, there is great interest in identifying and developing suitable lead-free alternatives.[131,132] Research remains in the early stages; there are many reports of moderate PLQY from lead-free perovskite or double perovskite nanomaterials.[133–137] Some of these were synthesized at room temperature; for example, Zhang et al. prepared $Cs_3Sb_2Br_9$ NCs that emit at 410 nm with PLQY = 46 % (Figure 17a),[138] while Leng et al. similarly synthesized $Cs_3Bi_2Br_9$ NCs with PLQY up to 19.4 % at the same wavelength.[139] Yang et al. reported that indium-doping of $Cs_2AgBiCl_6$ NCs changed the band-gap from indirect to direct, increasing the PLQY from 6.7 % to 36.6 % for emission around 570 nm (Figure 17b).[140] Similar to lead-based perovskite NCs, it is mainly solubility issues which have discouraged more room temperature syntheses for other lead-free materials. Therefore, adopting similar approaches to those covered earlier in this Progress Report should help tackle this.

However, despite improving PLQY, lead-free perovskite or double perovskite NCs have yet to demonstrate electroluminescence, so this remains an important challenge to prove their credentials as potential materials for LED applications. Ultimately, while they are unlikely to be an imminently viable option, if optoelectronic performance from lead-free perovskite nanocrystals can approach that of their lead-based counterparts in the future, there is no doubt that it would greatly enhance the commercially viability of the technology.

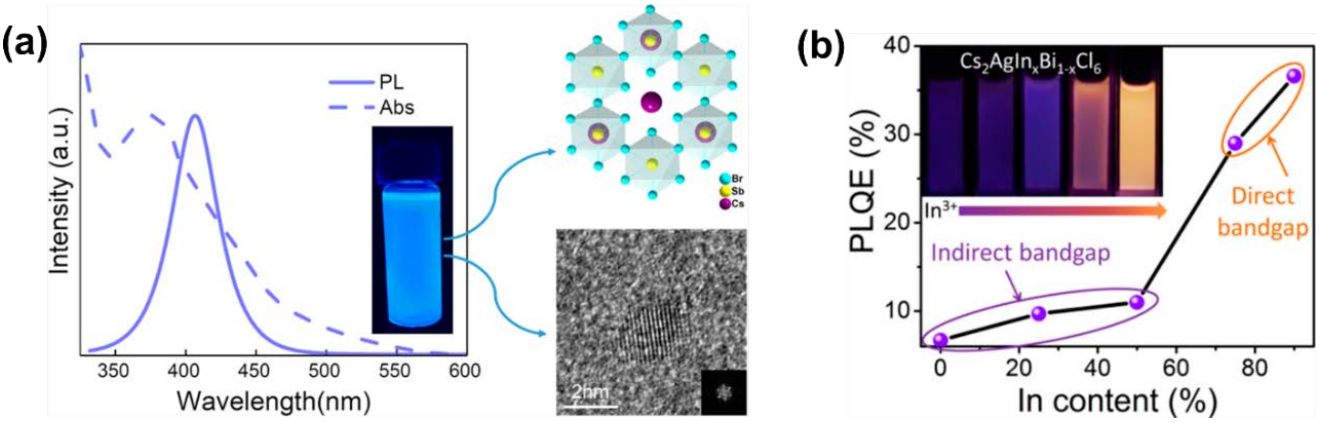

Figure 17. Direct band-gap lead-free perovskite nanocrystals synthesized at room temperature: (a) Optical characterization, photograph under UV light, structural diagram, and HRTEM image of $Cs_3Sb_2Br_9$ NCs (reproduced with permission from Ref.[138] Copyright 2017 American Chemical Society), and (b) PLQY as a function of indium content in $Cs_2AgIn_xBi_{1-x}Cl_6$ NCs, with the inset showing a photograph under UV light of the NC solutions corresponding to each data point (reproduced with permission from Ref.[140] Copyright 2018 American Chemical Society).

4.5 Green Solvent Selection

In addition to considering deposition and morphology when selecting solvents for NCs, it is crucial to consider industrial suitability. Given the current lack of lead-free perovskite NCs with comparable properties, it is particularly pertinent to ensure that the other chemicals utilized to prepare and deposit the lead-based NCs are as safe and sustainable as possible. Here we outline some potential greener alternative solvents that should be more appealing for industrial processes. The structures of the solvents replaced and those of some proposed replacements are displayed in Figure 18.

Starting with the polar solvent-based LARP method, there is one glaring issue. Although its low volatility is attractive to industry, dimethylformamide is a potent liver toxin and it is classified as a probable carcinogen. Furthermore, disposal of large quantities of DMF presents issues related to NO_x formation upon incineration.[141] Clearly, the adoption of the polar solvent-free methods discussed earlier would be ideal for eliminating the use of DMF. However, in the case that the polar solvent route is necessary or otherwise desired, dihydrolevoglucosenone (branded as Cyrene) is an appealing alternative. Cyrene is considered a green solvent, as it is derived through a two-step process from cellulose waste.[142,143] It is a dipolar aprotic solvent with similar physical and chemical properties to DMF, but displays no mutagenicity and low toxicity.[141] Its high viscosity (14.5 cP vs 0.92 cP for DMF) may inhibit its application for bulk perovskite film fabrication, but it has already proven to be a viable alternative to DMF for multiple applications in chemistry,[144,145] suggesting potential suitability for perovskite NC syntheses. Akkerman et al. previously replaced DMF successfully with isopropanol, however its volatility is less ideal for industrial-scale processes.[69]

Next, we address the non-polar solvents, which are used both as reaction media and dispersing agents for thin-film coating. Toluene is by far the most common non-polar reaction media for perovskite NCs,

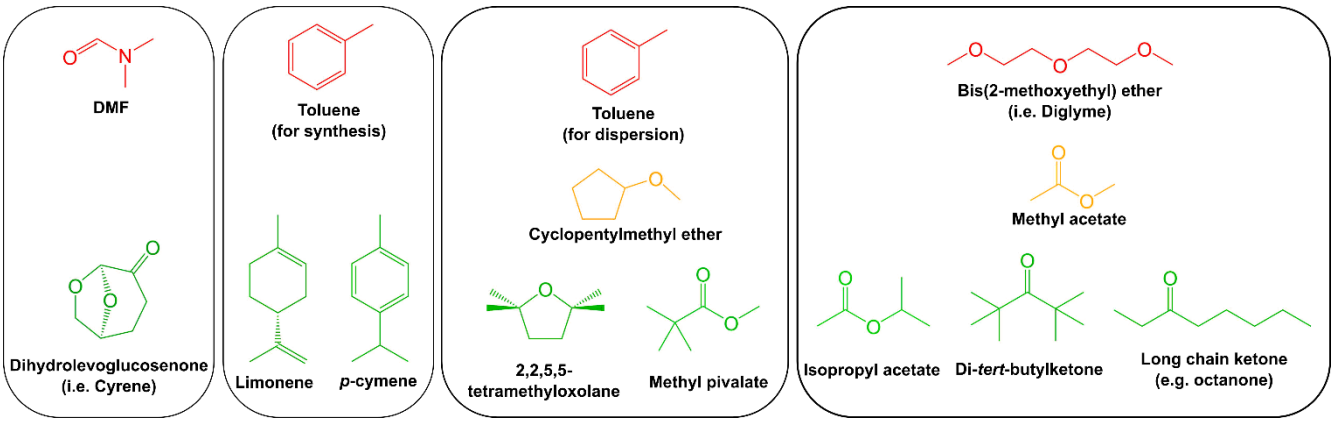

Figure 18. Potential green, more industrially suitable alternative solvents for each part of perovskite nanocrystal processing: synthesis, purification and dispersion. Structures shown in red are the current undesirable solvents, those shown in orange are more desirable solvents which still have some minor issues, while those in green are recommended suitable green solvents with no significant problems.

yet the toxicity of toluene is well-known – it is classified as a serious health hazard, suspected of organ and fertility damage. Furthermore, as NCs are typically isolated by centrifugation, there is no need to employ such a volatile solvent. The non-polar solvent limonene, and its derivative *p*-cymene, present similar properties but are non-toxic with higher boiling points (176 °C and 177 °C, respectively).[146,147] Furthermore, they are synthesized from citrus waste, so they are also considered sustainable, green solvents.[148] Therefore, investigating the compatibility of these, and other industrially attractive solvents, with the NC synthesis and purification process (i.e. solubility of ligands and miscibility with other solvents), would be a worthwhile endeavor.

Identifying appropriate dispersion solvents is more difficult, as there are more specific properties required. For example, toluene is often not used because it dissolves the typical polymer hole transport materials used in p-i-n structured LEDs (i.e. poly-TPD, PTAA). Toluene is normally replaced with alkane solvents such as octane, which are derived from fossil fuels. The replacement solvent must also have an appropriate boiling point for thin-film deposition; a low boiling point can lead to non-uniform films, while high boiling point solvents are difficult to fully dry, particularly as perovskite NCs films are sensitive to elevated temperatures. Ideally, the selected solvent should have a boiling point between 100 and 150 °C. One potential alternative is cyclopentyl methyl ether (CPME), which has the potential to be derived biogenically from furfural.[149] It has a very similar boiling point (106 °C) and polarity to toluene and is highly hydrophobic - a useful property for dispersing moisture-sensitive perovskite NCs.[150–152] CPME also has a narrow explosion range, however it has been classified as problematic because an anti-oxidant additive is required to prevent peroxide formation. There has been interesting recent research on syntheses of green, low toxicity quaternary ethers, such as 2,2,5,5-tetramethyloxolane (TMO),[153] whose lack of protons alpha to the oxygen prevents peroxide formation. There have also been investigations of the solvent properties of ketones and esters, which can be derived from potentially renewable feedstocks.[154] Multiple solvents were identified with very similar solubility parameters to toluene with boiling points between 100 and 115 °C, albeit with slightly higher polarity. These included the esters methyl pivalate, methyl butyrate and ethyl isobutyrate. It is probable that at least one of these solvents could facilitate the stable dispersion of perovskite NCs with strongly-bound ligands, and the deposition of smooth uniform films on a range of underlayers.

Lastly, we turn to the antisolvents used for NC purification. Diglyme, the antisolvent selected from a screening study by Hoshi et al., has exhibited reproductive toxicity from chronic exposure.[155] Thus, while acute toxicity is low, it would be preferable to find an alternative solvent. Fortunately, the ester solvents more typically employed are green and non-toxic.[156] The remaining issue to address is the volatility of the short esters used. Methyl and ethyl acetate have boiling points of 57 °C and 77 °C, respectively. Isopropyl acetate offers a better alternative, with a polarity between that of methyl and ethyl acetate but a boiling point of 89 °C. Although longer and more branched esters have higher boiling

points, their polarity is lower, thus they would not precipitate the nanocrystals from solution effectively. Other potentially appropriate green aprotic solvents, which have boiling points above 100 °C, are branched-chain ketones (e.g. methyl isobutyl ketone, or ditertbutylketone) or longer chain ketones (e.g. octanone).[141] These are slightly more polar but may be appropriate, particularly if NC solubility is high and ligands are strongly-bound.

5. Conclusion

Room temperature synthesis protocols for lead halide perovskite nanocrystals have been dramatically improved over the last 5 years. Polar solvent-free methods have been developed and can yield nanocrystals of comparable quality to high-temperature approaches. The initial weakly binding carboxylic acid/amine ligands have been replaced by a library of strongly binding ligands including quaternary ammonium halides, anionic ligands such as softer and multidentate carboxylic acids, phosphonic acids and sulfonic acids, and zwitterionic ligands, such as a long chain sulfobetaine and soy lecithin. Most of these novel ligands have not yet been utilized for room temperature syntheses but the methodology framework, particularly the use of bulky solubilizing agents such as tetraoctylammonium halides and trioctylphosphine oxide, should soon facilitate this.

In order to expedite progress towards commercialization, the organic tail of the ligand should be explored with the same rigor that the functional head groups have been. Highly branched "entropic" ligand chains could substantially enhance colloidal stability, such that highly concentrated nanocrystal dispersions can be reliably stored or transported for long periods of time. Functionalization of the ligand chain is another rarely investigated avenue, which can facilitate further chemistry such as cross-linking for improved environmental stability without compromising charge transport properties. The development of versatile room temperature metal doping protocols would provide a foundation for compositional engineering to optimize nanocrystal performance and stability, particularly for blue emission. Further research is also warranted into whether minor organic cation doping compromises the stability of $CsPbX_3$ NCs and the influence of alkali cation dopants/additives such as Rb^+ and K^+. Finally, we have proposed suitable green, industrially attractive solvent replacements for each stage of perovskite nanocrystal processing.

Together the research directions outlined herein could significantly boost the prospect of these exceptionally promising luminescent materials becoming a realistic option for industry.

6. Acknowledgments

A. A. M. B. gratefully acknowledges the Tizard studentship from the Faculty of Engineering and

Physical Sciences at University of Southampton.
This research was also supported by the National Research Foundation, Prime Minister's Office, Singapore, under its Competitive Research Program (CRP Award No. NRF-CRP14-2014-03).

7. Conflicts of Interest

The authors declare no conflicts of interest.

References

[1] A. Kojima, K. Teshima, Y. Shirai, T. Miyasaka, *Journal of the American Chemical Society* **2009**, 131(17), 6050.

[2] M.A. Green, A. Ho-Baillie, H.J. Snaith, *Nature Photonics* **2014**, 8(7), 506.

[3] T.B. Song, H. Zhou, C.C. Chen, Y.M. Yang, H. Zhao, Z. Hong, Y. Yang, N.D. Marco, Q. Chen, *Nano Today* **2015**, *10*(3), 355.

[4] N.K. Noel, S.D. Stranks, A. Abate, C. Wehrenfennig, S. Guarnera, A.A. Haghighirad, A. Sadhanala, G.E. Eperon, S.K. Pathak, M.B. Johnston, A. Petrozza, L.M. Herz, H.J. Snaith, *Energy and Environmental Science* **2014**, *7*(9), 3061.

[5] T.J. Jacobsson, J.P. Correa-Baena, M. Pazoki, M. Saliba, K. Schenk, M. Grätzel, A. Hagfeldt, *Energy and Environmental Science* **2016**, *9*(5), 1706.

[6] T.C. Sum, N. Mathews, *Energy and Environmental Science* **2014**, *7*(8), 2518.

[7] M. Grätzel, A. Hagfeldt, M. Saliba, W. Tress, J.P. Correa-Baena, A. Abate, T. Buonassisi, *Science* **2017**, *358*(6364), 739.

[8] P. Gao, M. Grätzel, M.K. Nazeeruddin, *Energy Environ. Sci.* **2014**, *7*(8), 2448.

[9] C.H.A. Li, Z. Zhou, P. Vashishtha, J.E. Halpert, *Chemistry of Materials* **2019**, *31*(16), 6003.

[10] M. Lu, Y. Zhang, S. Wang, J. Guo, W.W. Yu, A.L. Rogach, *Advanced Functional Materials* **2019**, *1902008*, 1.

[11] X. Zhao, J.D.A. Ng, R.H. Friend, Z.K. Tan, *ACS Photonics* **2018**, *5*(10), 3866.

[12] S.A. Veldhuis, T.C. Sum, M. Li, N. Mathews, P.P. Boix, S.G. Mhaisalkar, N. Yantara, *Advanced Materials* **2016**, *28*(32), 6804.

[13] N.K. Kumawat, D. Gupta, D. Kabra, *Energy Technology* **2017**, *5*(10), 1734.

[14] X.Y. Chin, D. Cortecchia, J. Yin, A. Bruno, C. Soci, *Nature Communications* **2015**, *6*(1), 7383.

[15] X. Liu, D. Yu, X. Song, H. Zeng, *Small* **2018**, *14*(36), 1801460.

[16] H. Zhu, Y. Fu, F. Meng, X. Wu, Z. Gong, Q. Ding, M.V. Gustafsson, M.T. Trinh, S. Jin, X.Y. Zhu, *Nature Materials* **2015**, *14*(6), 636.

[17] G. Li, M. Price, F. Deschler, *APL Materials* **2016**, *4*(9).

[18] Z. Zhu, Q. Sun, Z. Zhang, J. Dai, G. Xing, S. Li, X. Huang, W. Huang, *Journal of Materials Chemistry C* **2018**, *6*(38), 10121.

[19] W. Tian, H. Zhou, L. Li, *Small* **2017**, *13*(41).

[20] X. Wang, M. Li, B. Zhang, H. Wang, Y. Zhao, B. Wang, *Organic Electronics: physics, materials, applications* **2018**, *52*(September 2017), 172.

[21] H. Wang, D.H. Kim, *Chemical Society Reviews* **2017**, *46*(17), 5204.

[22] G. Xing, N. Mathews, S. Sun, S.S. Lim, Y.M. Lam, M. Gratzel, S. Mhaisalkar, T.C. Sum, *Science*

2013, *342*(6156), 344.

[23] G. Hodes, P.V. Kamat, *The Journal of Physical Chemistry Letters* **2015**, *6*(20), 4090.

[24] L.K. Ono, E.J. Juarez-Perez, Y. Qi, *ACS Applied Materials and Interfaces* **2017**, *9*(36), 30197.

[25] J. Kang, L.W. Wang, *Journal of Physical Chemistry Letters* **2017**, *8*(2), 489.

[26] H. Huang, M.I. Bodnarchuk, S.V. Kershaw, M.V. Kovalenko, A.L. Rogach, *ACS Energy Letters* **2017**, *2*(9), 2071.

[27] B. Saparov, D.B. Mitzi, *Chemical Reviews* **2016**, *116*(7), 4558.

[28] Q.A. Akkerman, G. Rainò, M.V. Kovalenko, L. Manna, *Nature Materials* **2018**, *17*(5), 394.

[29] M.V. Kovalenko, L. Protesescu, M.I. Bodnarchuk, *Science* **2017**, *358*(6364), 745.

[30] R.E. Brandt, V. Stevanović, D.S. Ginley, T. Buonassisi, *MRS Communications 2015*, *5*(2), 265.

[31] S.D. Stranks, R.L. Hoye, D. Di, R.H. Friend, F. Deschler, *Advanced Materials* **2018**, *1803336*.

[32] G. Xing, B. Wu, X. Wu, M. Li, B. Du, Q. Wei, J. Guo, E.K. Yeow, T.C. Sum, W. Huang, *Nature Communications* **2017**, *8*, 14558.

[33] M. Green, *Journal of Materials Chemistry* **2010**, *20*(28), 5797.

[34] Y. Yang, H. Qin, X. Peng, *Nano Letters* **2016**, *16*(4), 2127.

[35] T. Chiba, Y. Hayashi, H. Ebe, K. Hoshi, J. Sato, S. Sato, Y.J. Pu, S. Ohisa, J. Kido, *Nature Photonics* **2018**, *12*(11), 681.

[36] X.Y. Chin, A. Perumal, A. Bruno, N. Yantara, S.A. Veldhuis, L. Martínez-Sarti, B. Chandran, V. Chirvony, A.S.Z. Lo, J. So, C. Soci, M. Grätzel, H.J. Bolink, N. Mathews, S.G. Mhaisalkar, *Energy and Environmental Science* **2018**, *11*(7), 1770.

[37] J. Song, T. Fang, J. Li, L. Xu, F. Zhang, B. Han, Q. Shan, H. Zeng, *Advanced Materials* **2018**, *30*(50), 1.

[38] D.P. Nenon, K. Pressler, W.T. Osowiecki, J.H. Olshansky, A.P. Alivisatos, L.W. Wang, J. Kang, B.A. Koscher, M.A. Koc, *Journal of the American Chemical Society* **2018**, *140*(50), 17760.

[39] S.R. Smock, T.J. Williams, R.L. Brutchey, *Angewandte Chemie - International Edition* **2018**, *90089*, 11711.

[40] J.H. Park, A.Y. Lee, J.C. Yu, Y.S. Nam, Y. Choi, J. Park, M.H. Song, *ACS Applied Materials and Interfaces* **2019**, *11*(8), 8428.

[41] J. Song, J. Li, L. Xu, J. Li, F. Zhang, B. Han, Q. Shan, H. Zeng, *Advanced Materials* **2018**, *30*(30), 1800764.

[42] Z. Zhang, Y. Jin, Y. Niu, H. Qin, F. Zhao, X. Peng, H. Cao, T. Fu, X. Dai, M. Jiang, L. Lin, Y. Yang, *Nano Letters* **2016**, *16*(4), 2133.

[43] T. Wang, L. Xu, J. Chen, J. Li, J. Song, B. Han, H. Zeng, Q. Shan, Y. Dong, B. Cai, J. Xue, *Advanced Materials* **2016**, *29*(5), 1603885.

[44] T. Chiba, K. Hoshi, Y.J. Pu, Y. Takeda, Y. Hayashi, S. Ohisa, S. Kawata, J. Kido, *ACS Applied*

Materials and Interfaces **2017**, *9*(21), 18054.

[45] K. Hoshi, T. Chiba, J. Sato, Y. Hayashi, Y. Takahashi, H. Ebe, S. Ohisa, J. Kido, *ACS Applied Materials and Interfaces* **2018**, *10*(29), 24607.

[46] L. Protesescu, S. Yakunin, M.I. Bodnarchuk, A. Walsh, F. Krieg, R. Caputo, C.H. Hendon, R.X. Yang, M.V. Kovalenko, *Nano Letters* **2015**, *15*(6), 3692.

[47] S. Wei, Y. Yang, X. Kang, L. Wang, L. Huang, D. Pan, *Inorganic Chemistry* **2017**, *56*(5), 2596.

[48] H. Zhong, H. Huang, F. Zhang, J. Han, B. Zou, X. gang Wu, C. Chen, X. Hu, Y. Dong, *ACS Nano* **2015**, *9*(4), 4533.

[49] A. Perumal, S. Shendre, M. Li, Y.K.E. Tay, V.K. Sharma, S. Chen, Z. Wei, Q. Liu, Y. Gao, P.J.S. Buenconsejo, S.T. Tan, C.L. Gan, Q. Xiong, T.C. Sum, H.V. Demir, *Scientific Reports* **2016**, *6*(1), 36733.

[50] H. Chen, L. Fan, R. Zhang, C. Bao, H. Zhao, W. Xiang, W. Liu, G. Niu, R. Guo, L. Zhang, L. Wang, *Advanced Optical Materials* **2020**, 1901390.

[51] Y.H. Kim, G.H. Lee, Y.T. Kim, C. Wolf, H.J. Yun, W. Kwon, C.G. Park, T.W. Lee, *Nano Energy* **2017**, 38(April), 51.

[52] Y.L. Tong, Y.W. Zhang, K. Ma, R. Cheng, F. Wang, S. Chen, *ACS Applied Materials and Interfaces* **2018**, *10*(37), 31603.

[53] R.J. Sutton, G.E. Eperon, L. Miranda, E.S. Parrott, B.A. Kamino, J.B. Patel, M.T. Hörantner, M.B. Johnston, A.A. Haghighirad, D.T. Moore, H.J. Snaith, *Advanced Energy Materials* **2016**, *6*(8), 1502458.

[54] M. Salado, L. Calio, R. Berger, S. Kazim, S. Ahmad, *Physical Chemistry Chemical Physics* **2016**, *18*(39), 27148.

[55] R. Cheacharoen, R. Beal, K. Bush, A. Bowring, T. Leijtens, M.D. McGehee, *Journal of Materials Chemistry A* **2017**, *5*(23), 11483.

[56] S.H. Turren-Cruz, A. Hagfeldt, M. Saliba, *Science* **2018**, *362*(6413), 449.

[57] M. Saliba, T. Matsui, J.Y. Seo, K. Domanski, J.P. Correa-Baena, M.K. Nazeeruddin, S.M. Zakeeruddin, W. Tress, A. Abate, A. Hagfeldt, M. Grätzel, *Energy and Environmental Science* **2016**, *9*(6), 1989.

[58] M. Deepa, M. Salado, L. Calio, S. Kazim, S.M. Shivaprasad, S. Ahmad, *Physical Chemistry Chemical Physics* **2017**, *19*(5), 4069.

[59] M. Liu, H. Zhang, D. Gedamu, P. Fourmont, H. Rekola, A. Hiltunen, S.G. Cloutier, R. Nechache, A. Priimagi, P. Vivo, *Small* **2019**, *1900801*, 1.

[60] N. Pradhan, *The Journal of Physical Chemistry Letters* **2019**, *10*, 5847.

[61] J. Shamsi, A.S. Urban, M. Imran, L.D. Trizio, L. Manna, *Chemical Reviews* **2019**, *119*(5), 3296.

[62] S.A. Kulkarni, S.G. Mhaisalkar, N. Mathews, P.P. Boix, *Small Methods* **2018**, *3*(1), 1800231.

[63] X. Li, Y. Wu, S. Zhang, B. Cai, Y. Gu, J. Song, H. Zeng, *Advanced Functional Materials* **2016**, *26*(15), 2435.

[64] S.A. Veldhuis, Y.F. Ng, R. Ahmad, A. Bruno, N.F. Jamaludin, B. Damodaran, N. Mathews, S.G. Mhaisalkar, *ACS Energy Letters* **2018**, *3*(3), 526.

[65] J. Li, D. Yim, W.D. Jang, J. Yoon, *Chemical Society Reviews* **2017**, *46*(9), 2437.

[66] E. Moyen, A. Kanwat, S. Cho, H. Jun, R. Aad, J. Jang, *Nanoscale* **2018**, *10*(18), 8591.

[67] E. Moyen, H. Jun, H.M. Kim, J. Jang, *ACS Applied Materials and Interfaces* **2018**, *10*(49), 42647.

[68] Y. Zou, M. Ban, W. Cui, Q. Huang, C. Wu, J. Liu, H. Wu, T. Song, B. Sun, *Advanced Functional Materials* **2017**, *27*(1).

[69] Q.A. Akkerman, M. Gandini, F.D. Stasio, P. Rastogi, F. Palazon, G. Bertoni, J.M. Ball, M. Prato, A. Petrozza, L. Manna, *Nature Energy* **2017**, *2*(2), 16194.

[70] F. Ye, H. Zhang, W. Li, Y. Yan, J. Cai, R.S. Gurney, A.J. Pearson, D. Liu, T. Wang, *Small Methods* **2019**, *3*(3), 1800489.

[71] J. Pan, Y. Shang, J. Yin, M.D. Bastiani, W. Peng, I. Dursun, L. Sinatra, A.M. El-Zohry, M.N. Hedhili, A.H. Emwas, O.F. Mohammed, Z. Ning, O.M. Bakr, *Journal of the American Chemical Society* **2018**, *140*(2), 562.

[72] H. Wu, Y. Zhang, M. Lu, X. Zhang, C. Sun, T. Zhang, V.L. Colvin, W.W. Yu, *Nanoscale* **2018**, *10*(9), 4173.

[73] A.A.M. Brown, T.J.N. Hooper, S.A. Veldhuis, X.Y. Chin, A. Bruno, P. Vashishtha, J.N. Tey, L. Jiang, B. Damodaran, S.H. Pu, S.G. Mhaisalkar, N. Mathews, *Nanoscale* **2019**, *11*(25), 12370.

[74] M. Imran, V. Caligiuri, M. Wang, L. Goldoni, M. Prato, R. Krahne, L.D. Trizio, L. Manna, *Journal of the American Chemical Society* **2018**, *140*(7), 2656.

[75] D. Yang, X. Li, W. Zhou, S. Zhang, C. Meng, Y. Wu, Y. Wang, H. Zeng, *Advanced Materials* **2019**, *1900767*, 1900767.

[76] B. Zhang, L. Goldoni, J. Zito, Z. Dang, G. Almeida, F. Zaccaria, J. de Wit, I. Infante, L.D. Trizio, L. Manna, *Chemistry of Materials* **2019**, *31*(21), 9140

[77] J-N. Yang, Y. Song, J-S. Yao, K-H. Wang, J-J. Wang, B-S. Zhu, M-M. Yao, S.U. Rahman, Y-F. Lan, F-J. Fan, H-B. Yao, *Journal of the American Chemical Society* **2020**, *142*(6), 2956-2967.

[78] Y. Hassan, O.J. Ashton, J.H. Park, G. Li, N. Sakai, B. Wenger, A.A. Haghighirad, N.K. Noel, M.H. Song, B.R. Lee, R.H. Friend, H.J. Snaith, *Journal of the American Chemical Society* **2019**, *141*(3), 1269.

[79] P. Todorović, D. Ma, B. Chen, R. Quintero-Bermudez, M.I. Saidaminov, Y. Dong, Z-H. Lu, E.H. Sargent, *Advanced Optical Materials* **2019**, *1901440*, 1901440.

[80] Y. Tan, Y. Zou, L. Wu, Q. Huang, D. Yang, M. Chen, M. Ban, C. Wu, T. Wu, S. Bai, T. Song, Q. Zhang, B. Sun, *ACS Applied Materials and Interfaces* **2018**, *10*(4), 3784.

[81] Y. Dong, T. Qiao, D. Kim, D. Parobek, D. Rossi, D.H. Son, *Nano Letters* **2018**, *18*(6), 3716.

[82] F. Ambroz, W. Xu, S. Gadipelli, D.J. Brett, C.T. Lin, C. Contini, M.A. McLachlan, J.R. Durrant, I.P. Parkin, T.J. Macdonald, *Particle and Particle Systems Characterization* **2019**, *1900391*, 1.

[83] W.J. Mir, A. Swarnkar, A. Nag, *Nanoscale* **2019**, *11*(10), 4278.

[84] J. De Roo, M. Ibáñez, P. Geiregat, G. Nedelcu, I.V. Driessche, Z. Hens, W. Walravens, J.C. Martins, J. Maes, M.V. Kovalenko, *ACS Nano* **2016**, *10*(2), 2071.

[85] J. Pan, L.N. Quan, Y. Zhao, W. Peng, B. Murali, S.P. Sarmah, M. Yuan, L. Sinatra, N.M. Alyami, J. Liu, E. Yassitepe, Z. Yang, O. Voznyy, R. Comin, M.N. Hedhili, O.F. Mohammed, Z.H. Lu, D.H. Kim, E.H. Sargent, O.M. Bakr, *Advanced Materials* **2016**, *28*(39), 8718.

[86] Y. Shynkarenko, M.I. Bodnarchuk, C. Bernasconi, Y. Berezovska, V. Verteletskyi, S.T. Ochsenbein, M.V. Kovalenko, *ACS Energy Letters* **2019**, *4*(11), 2703.

[87] F. Yang, H. Chen, R. Zhang, X. Liu, W. Zhang, J. Zhang, F. Gao, L. Wang, *Advanced Functional Materials* **2020**, *1908760*.

[88] G. Almeida, O.J. Ashton, L. Goldoni, D. Maggioni, U. Petralanda, N. Mishra, Q.A. Akkerman, I. Infante, H.J. Snaith, L. Manna, *Journal of the American Chemical Society* **2018**, *140*(44), 14878.

[89] L. Zhao, K.M. Lee, K. Roh, S.U.Z. Khan, B.P. Rand, *Advanced Materials* **2019**, *31*(2), 1.

[90] D. Yang, X. Li, W. Zhou, S. Zhang, C. Meng, Y. Wu, Y. Wang, H. Zeng, *Advanced Materials* **2019**, *1900767*.

[91] F. Ye, H. Zhang, P. Wang, J. Cai, L. Wang, D. Liu, T. Wang, *Chemistry of Materials* **2020**.

[92] F. Krieg, S.T. Ochsenbein, S. Yakunin, S.T. Brinck, P. Aellen, A. Süess, B. Clerc, D. Guggisberg, O. Nazarenko, Y. Shynkarenko, S. Kumar, C.J. Shih, I. Infante, M.V. Kovalenko, *ACS Energy Letters* **2018**, *3*(3), 641.

[93] S.T. Ochsenbein, F. Krieg, Y. Shynkarenko, G. Rainò, M.V. Kovalenko, *ACS Applied Materials and Interfaces* **2019**, *11*(24), 21655.

[94] F. Krieg, Q.K. Ong, M. Burian, G. Rainò, D. Naumenko, H. Amenitsch, A. Süess, M.J. Grotevent, F. Krumeich, M.I. Bodnarchuk, I. Shorubalko, F. Stellacci, M.V. Kovalenko, *Journal of the American Chemical Society* **2019**, *141*(50), 19839.

[95] J. De Roo, Z. Zhou, J. Wang, L. Deblock, A.J. Crosby, J.S. Owen, S.S. Nonnenmann, *Chemistry of Materials* **2018**, *30*(21), 8034.

[96] J. Tong, J. Wu, W. Shen, Y. Zhang, Y. Liu, T. Zhang, S. Nie, Z. Deng, *ACS Applied Materials and Interfaces* **2019**, *11*(9), 9317.

[97] Q. Zhong, M. Cao, H. Hu, D. Yang, M. Chen, P. Li, L. Wu, Q. Zhang, *ACS Nano* **2018**, *12*(8), 8579.

[98] H. Sun, Z. Yang, M. Wei, W. Sun, X. Li, S. Ye, Y. Zhao, H. Tan, E.L. Kynaston, T.B. Schon, H. Yan, Z.H. Lu, G.A. Ozin, E.H. Sargent, D.S. Seferos, *Advanced Materials* **2017**, *29*(34), 1.

[99] A. Kanwat, E. Moyen, S. Cho, J. Jang, *ACS Applied Materials & Interfaces* **2018**, *10*(19), 16852.

[100] Y. Shi, J. Xi, T. Lei, F. Yuan, J. Dai, C. Ran, H. Dong, B. Jiao, X. Hou, Z. Wu, *ACS Applied Materials and Interfaces* **2018**, *10*(11), 9849.

[101] Y. Liu, G. Pan, R. Wang, H. Shao, H. Wang, W. Xu, H. Cui, H. Song, *Nanoscale* **2018**, *10*(29), 14067.

[102] S. Kafashi, M.R. Yaftian, A.A. Zamani, *Journal of Solution Chemistry* **2015**, *44*(9), 1798.

[103] S.C. Erwin, L. Zu, M.I. Haftel, A.L. Efros, T.A. Kennedy, D.J. Norris, *Nature* **2005**, *436*(7047), 91.

[104] D.J. Norris, A.L. Efros, S.C. Erwin, *Science* **2008**, *319*(5871), 1776.

[105] A. Dutta, R.K. Behera, N. Pradhan, *ACS Energy Letters* **2019**, *4*(4), 926.

[106] G.H. Ahmed, J. Yin, O.M. Bakr, O.F. Mohammed, *Journal of Chemical Physics* **2020**, *152*(2).

[107] A. Shapiro, M.W. Heindl, F. Horani, M.H. Dahan, J. Tang, Y. Amouyal, E. Lifshitz, *The Journal of Physical Chemistry C* **2019**.

[108] C. Bi, S. Wang, Q. Li, S.V. Kershaw, J. Tian, A.L. Rogach, *Journal of Physical Chemistry Letters* **2019**, *10*(5), 943.

[109] J.Y. Woo, Y. Kim, J. Bae, T.G. Kim, J.W. Kim, D.C. Lee, S. Jeong, *Chemistry of Materials* **2017**, *29*(17), 7088.

[110] J. Park, Y. Kim, S. Ham, J.Y. Woo, T. Kim, S. Jeong, D. Kim, *Nanoscale* **2020**, *12*(3), 1563.

[111] W. van der Stam, J.J. Geuchies, T. Altantzis, K.H.W. van den Bos, J.D. Meeldijk, S.V. Aert, S. Bals, D. Vanmaekelbergh, C. de Mello Donega, *Journal of the American Chemical Society* **2017**, *139*(11), 4087.

[112] N. Mondal, A. De, A. Samanta, *ACS Energy Letters* **2019**, *4*(1), 32.

[113] G. Zhong, M. Liu, J. Miao, H. Meng, X. Xu, C. Shen, C. Wang, K. Li, Y. Yin, *Advanced Science* **2017**, *4*(11), 1700335.

[114] B. Luo, F. Li, K. Xu, Y. Guo, Y. Liu, Z. Xia, J.Z. Zhang, *Journal of Materials Chemistry C* **2019**, *7*(10), 2781.

[115] M.R. Filip, F. Giustino, *Journal of Physical Chemistry C* **2016**, *120*(1), 166.

[116] P. Vashishtha, J.E. Halpert, *Chemistry of Materials* **2017**, *29*(14), 5965.

[117] W. Liu, Q. Lin, H. Li, K. Wu, I. Robel, J.M. Pietryga, V.I. Klimov, *Journal of the American Chemical Society* **2016**, *138*(45), 14954.

[118] D. Parobek, Y. Dong, T. Qiao, D.H. Son, *Chemistry of Materials* **2018**, *30*(9), 2939.

[119] P.K. R., D. Acharya, P. Jain, K. Gahlot, A. Yadav, A. Camellini, M. Zavelani-Rossi, G. Cerullo, C. Narayana, S. Narasimhan, R. Viswanatha, *ACS Energy Letters* **2020**, pp. 353–359.

[120] S. Hou, M.K. Gangishetty, Q. Quan, D.N. Congreve, *Joule* **2018**, *2*(11), 2421.

[121] A. Mahata, D. Meggiolaro, F.D. Angelis, *Journal of Physical Chemistry Letters* **2019**, *10*(8), 1790-

1798.

[122] H. Zhu, K. Miyata, Y. Fu, J. Wang, P.P. Joshi, D. Niesner, K.W. Williams, S. Jin, X.Y. Zhu, *Science* **2016**, *353*(6306), 1409.

[123] M. Grätzel, P. Péchy, A. Hofstetter, D.J. Kubicki, L. Emsley, S.M. Zakeeruddin, D. Prochowicz, *Journal of the American Chemical Society* **2017**, *139*(29), 10055.

[124] D.H. Fabini, T.A. Siaw, C.C. Stoumpos, G. Laurita, D. Olds, K. Page, J.G. Hu, M.G. Kanatzidis, S. Han, R. Seshadri, *Journal of the American Chemical Society* **2017**, *139*(46), 16875.

[125] M. Hao, Y. Bai, S. Zeiske, L. Ren, J. Liu, Y. Yuan, N. Zarrabi, N. Cheng, M. Ghasemi, P. Chen, M. Lyu, D. He, J.H. Yun, Y. Du, Y. Wang, S. Ding, A. Armin, P. Meredith, G. Liu, H.M. Cheng, L. Wang, *Nature Energy* **2020**, *5*(1), 79.

[126] Y. Galagan, *Journal of Physical Chemistry Letters* **2018**, *9*(15), 4326.

[127] N.G. Park, K. Zhu, *Nature Reviews Materials* **2020**.

[128] V. Prakasam, D. Tordera, F.D. Giacomo, R. Abbel, A. Langen, G. Gelinck, H.J. Bolink, *Journal of Materials Chemistry C* **2019**.

[129] W. Ke, M.G. Kanatzidis, *Nature Communications* **2019**, *10*(1), 1.

[130] S. Ghosh, B. Pradhan, *ChemNanoMat* **2019**, pp. 300–312.

[131] J. Sun, J. Yang, J.I. Lee, J.H. Cho, M.S. Kang, *Journal of Physical Chemistry Letters* **2018**, *9*(7), 1573.

[132] S. Khalfin, Y. Bekenstein, *Nanoscale* **2019**, *11*(18), 8665.

[133] M.M. Yao, L. Wang, J.S. Yao, K.H. Wang, C. Chen, B.S. Zhu, J.N. Yang, J.J. Wang, W.P. Xu, Q. Zhang, H.B. Yao, *Advanced Optical Materials* **2020**, *1901919*, 2.

[134] Y. Liu, Y. Jing, J. Zhao, Q. Liu, Z. Xia, *Chemistry of Materials* **2019**, *31*(9), 3333.

[135] F. Locardi, M. Cirignano, D. Baranov, Z. Dang, M. Prato, F. Drago, M. Ferretti, V. Pinchetti, M. Fanciulli, S. Brovelli, L.D. Trizio, L. Manna, *Journal of the American Chemical Society* **2018**, *140*(40), 12989.

[136] R. Chiara, Y.O. Ciftci, V.I. Queloz, M.K. Nazeeruddin, G. Grancini, L. Malavasi, *Journal of Physical Chemistry Letters* **2020**, *11*(3), 618.

[137] J.L. Xie, Z.Q. Huang, B. Wang, W.J. Chen, W.X. Lu, X. Liu, J.L. Song, *Nanoscale* **2019**, *11*(14), 6719.

[138] J. Zhang, Y. Yang, H. Deng, U. Farooq, X. Yang, J. Khan, J. Tang, H. Song, *ACS Nano* **2017**, *11*(9), 9294.

[139] M. Leng, Y. Yang, K. Zeng, Z. Chen, Z. Tan, S. Li, J. Li, B. Xu, D. Li, M.P. Hautzinger, Y. Fu, T. Zhai, L. Xu, G. Niu, S. Jin, J. Tang, *Advanced Functional Materials* **2018**, *28*(1), 1.

[140] B. Yang, X. Mao, F. Hong, W. Meng, Y. Tang, X. Xia, S. Yang, W. Deng, K. Han, *Journal of the American Chemical Society* **2018**, *140*(49), 17001.

[141] J. Zhang, G.B. White, M.D. Ryan, A.J. Hunt, M.J. Katz, *ACS Sustainable Chemistry and Engineering* **2016**, *4*(12), 7186.

[142] J. Sherwood, M.D. Bruyn, A. Constantinou, L. Moity, C.R. McElroy, T.J. Farmer, T. Duncan, W. Raverty, A.J. Hunt, J.H. Clark, *Chemical Communications* **2014**, *50*(68), 9650.

[143] J.E. Camp, *ChemSusChem* **2018**, *11*(18), 3048.

[144] R. Poon, I. Zhitomirsky, *Colloid and Interface Science Communications* **2020**, *34*(11), 100226.

[145] K. Pan, Y. Fan, T. Leng, J. Li, Z. Xin, J. Zhang, L. Hao, J. Gallop, K.S. Novoselov, Z. Hu, *Nature Communications* **2018**, *9*(1).

[146] S. Chemat, V. Tomao, F. Chemat, *Green Solvents I: Properties and Applications in Chemistry* 2012.

[147] J.H. Clark, D.J. MacQuarrie, J. Sherwood, *Green Chemistry* **2012**, *14*(1), 90.

[148] M. Lamarche, M.T. Dang, J. Lefebvre, J.D. Wuest, S. Roorda, *ACS Sustainable Chemistry and Engineering* **2017**, *5*(7), 5994.

[149] K. Watanabe, N. Yamagiwa, Y. Torisawa, *Organic Process Research and Development* **2007**, *11*(2), 251.

[150] V. Antonucci, J. Coleman, J.B. Ferry, N. Johnson, M. Mathe, J.P. Scott, J. Xu, *Organic Process Research and Development* **2011**, *15*(4), 939.

[151] C.M. Abreu, P. Maximiano, T. Guliashvili, J. Nicolas, A.C. Serra, J.F. Coelho, *RSC Advances* **2016**, *6*(9), 7495.

[152] G. de Gonzalo, A.R. Alcántara, P.D. de María, *ChemSusChem* **2019**, *12*(10), 2083.

[153] F. Byrne, B. Forier, G. Bossaert, C. Hoebers, T.J. Farmer, J.H. Clark, A.J. Hunt, *Green Chemistry* **2017**, *19*(15), 3671.

[154] F.P. Byrne, B. Forier, G. Bossaert, C. Hoebers, T.J. Farmer, A.J. Hunt, *Green Chemistry* **2018**, *20*(17), 4003.

[155] S. Tang, H. Zhao, *RSC Advances* **2014**, *4*(22), 11251.

[156] F.P. Byrne, S. Jin, G. Paggiola, T.H.M. Petchey, J.H. Clark, T.J. Farmer, A.J. Hunt, C.R. McElroy, J. Sherwood, *Sustainable Chemical Processes* **2016**, *4*(1), 7.